STRESS ANALYSIS AND LIFE PREDICTION OF TURBINE BLADES

A Thesis Submitted

in Partial Fulfilment of the Requirements

for the Degree of

MASTER OF TECHNOLOGY

by

SIDHARTH

to the

DEPARTMENT OF MECHANICAL ENGINEERING

INDIAN INSTITUTE OF TECHNOLOGY KANPUR

MARCH, 1992

ME-1992-M-SID-STR

11 MAY 1992
CENTRAL LIBRARY
I I T KANPUR
Acc. No. A.113372

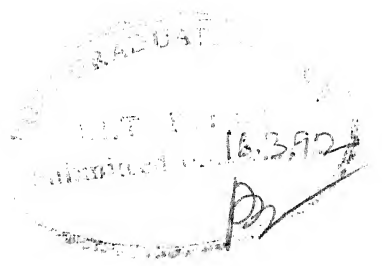

C E R T I F I C A T E

It is certified that the work contained in this thesis entitled " **STRESS ANALYSIS AND LIFE PREDICTION OF TURBINE BLADES** ", by Sidharth, has been carried out under my supervision and that this work has not been submitted elsewhere for a degree.

March, 1992

Nalinaksh S Vyas
Assistant Professor
Department of Mechanical Engineering
Indian Institute of Technology
Kanpur 208016

A B S T R A C T

This study is concerned with the development of an analytical code for Dynamic Stress Analysis and Fatigue Life Prediction of Turbomachinery Blades. Emerging blade technologies are finding it increasingly essential to correlate blade vibrations to blade fatigue in order to assess the residual life of existing blading and for the development of newer blade designs.

On the basis of previously done available work an attempt has been made to refine the approach for stress analysis by incorporating the crucially important aspect of nonlinearity in damping. The numerical procedure developed for estimation of stresses under nonlinear damping is presented.

A life prediction algorithm, based on the strain-life and fracture mechanics concepts to account for the blade fatigue phenomenon involving crack initiation and crack growth, has been developed as an improvement upon the conventional stress based approach.

The stress analysis code coupled with the life algorithm forms an overall package.

A C K N O W L E D G E M E N T S

I express my deep gratitude to Dr. N S Vyas, my thesis supervisor, for his valuable guidance and constant encouragement throughout this work. I have the highest regards for his openness to discussions, patience towards my riders, granting freedom to work independently and constructive criticism from time to time. Working with him has indeed been an enriching experience for me.

I gratefully acknowledge the help rendered by V A Pankhawala, M N Jha and P Agarwal towards the preparation of this document.

I express my thanks to B Ravindra and Mr. M M Singh, who have been supportive throughout.

Piyush and Yadav have been my think tank; Jha and Subodh, the friendly neighbourhood; and they have shared my joys and sorrows during this period. The SMD gang and other Hall IV inmates have provided me memories to cherish, a long time to come.

Last, but not the least, my parents deserve my deepest appreciation for their love and support.

S I D H A R T H

Indian Institute of Technology, Kanpur

March, 1992

CONTENTS

NOMENCLATURE

A	Area of cross-section
B	Body force distribution
a	Crack length
a,b	Coefficients in trigonometric series of forcing functions
a_i	Initial crack length
a_f	Final Crack length
b	Fatigue strength exponent ; width of the plate
C	Torsional stiffness
c	Fatigue ductility exponent
D_n	Depth of notch
E	Modulus of Elasticity
e	Engineering normal strain
F	Correction factor for stress intensity factor
F_x, F_y	Forcing functions
f	Shape function for bending deflections
$\overline{f}$	Shape function for angular deflections
H_{m_k}	mth harmonic response in the kth mode
h	Shape function for bending and twisting moments
$I_{x_1x_1}$	Second moment of area about $X_1 - X_1$ axis
$I_{y_1y_1}$	Second moment of area about $Y_1 - Y_1$ axis
$I_{x_1y_1}$	Product moment of area about $X_1 - Y_1$ axis
I_{cg}	Moment of inertia per unit length

I_R	Reissner's functional
k	Strength coefficient under monotonic loading
k'	Strength coefficient under cyclic loading
k_c	Fracture toughness
k_f	Fatigue stress concentration factor
k_{max}	Maximum stress intensity factor
k_{min}	Minimum stress intensity factor
k_t	Theoretical stress concentration factor
k_{IC}	Plain strain fracture toughness
k_ϵ	Strain concentration factor
k_σ	True stress concentration factor
ΔK	Stress intensity range = $k_{max} - k_{min}$
L	Reissner's dynamic functional
l	Blade length
l_t	Transition crack length
M	Moment
M_x, M_y	Moment in x and y directions
m	Harmonic number ; material constant
NPF	Nozzle passing frequency
N_i	Initiation life
N_p	Propagation life
N_t	Total life
n	Strain hardening exponent under monotonic loading
n'	Strain hardening exponent under cyclic loading
n_s	Number of nozzles
p_k	Natural frequency in the kth mode
Q	Forcing vector

R	Disc radius
R_f	Endurance limit modifying factor
r_x, r_y	Coordinates of the centre of flexure
S	Nominal stress
S_e	Endurance limit for 10^3 cycles
S_e'	Endurance limit for N cycles
S_u	Ultimate tensile strength
S_y	Yield strength
s	Surface area
T	Kinetic energy
T_i	Traction force in the i-th direction
T_θ	Twisting moment
t	time
$[U]$	Modal matrix
U_o^*	Complementary energy density function
u_i	Displacement in the i-th direction
v	Volume
xx, yy	Coordinate axes through centre of flexure
x_1x_1, y_1y_1	Coordinate axes through centroid
z	Distance along the blade length
α	Angular acceleration
ϵ	Normal strain
ϵ_e	Elastic strain
ϵ_{ij}	Strain
ϵ_p	Plastic strain
ϵ_f'	Fatigue ductility coefficient

$\Delta\epsilon$	Strain range
$\Delta\epsilon_e$	Elastic strain range
$\Delta\epsilon_p$	Plastic strain range
$\eta\eta, \xi\xi$	Coordinate axes, refer Fig. 3.1
η	Generalised coordinate
ν	Nozzle passing frequency
ζ	Modal damping ratio
ρ	Mass density
σ	Normal stress
$\sigma_1, \sigma_2, \sigma_3$	Principal stresses
σ_a	Alternating stress
σ_{af}, σ_{mf}	Failure values of mean and alternating stress
σ_m	Total mean stress
σ_{mv}	Mean stress due to zeroth NPF component
σ_z	Bending stress
$\Delta\sigma$	Stress range
τ_{ij}	Stress
τ_{xx}, τ_{yy}	Shear stresses
ϕ	Stagger angle
ω	Angular frequency
$(')$	Denotes differentiation with respect to z
$(\dot{})$	Denotes differentiation with respect to t
XX, YY	Principal axes
Ψ_z	Pretwist angle

LIST OF FIGURES

LIST OF TABLES

CHAPTER 1

INTRODUCTION

Vibration induced fatigue is a problem of major concern in turbomachinery blading. With ever increasing demand for high speed turbines, blade vibration and fatigue has become an important subject of study. Blade behaviour is strongly influenced by the mean and alternating stresses, experienced during operation, by the elastic and fatigue properties of the blade material and the chemistry of the operating environment. The critical aspect of the problem constitutes occurence of large dynamic stresses, due to resonant or near resonant vibration at an integral order of engine speed, when a component of the vibrating blade matches in both time and space a corresponding pattern in the gas/steam stream caused by the nozzle flow field.

Blade fatigue usually initiates in a region of high stress at some structural and/or metallurgical discontinuity. The earlier practice had been to avoid fatigue failure by tuning the blade to operate away from the natural frequencies. However, in a typical turbomachine this may not always be possible, for it may have three or four rotors, each having several stages and the turbine may altogether have many blades with different characteristics. Dynamic stress analysis of the blade, therefore assumes importance.

Fig. 1.1 summarises the steps involved in the analysis of a turbine blade.

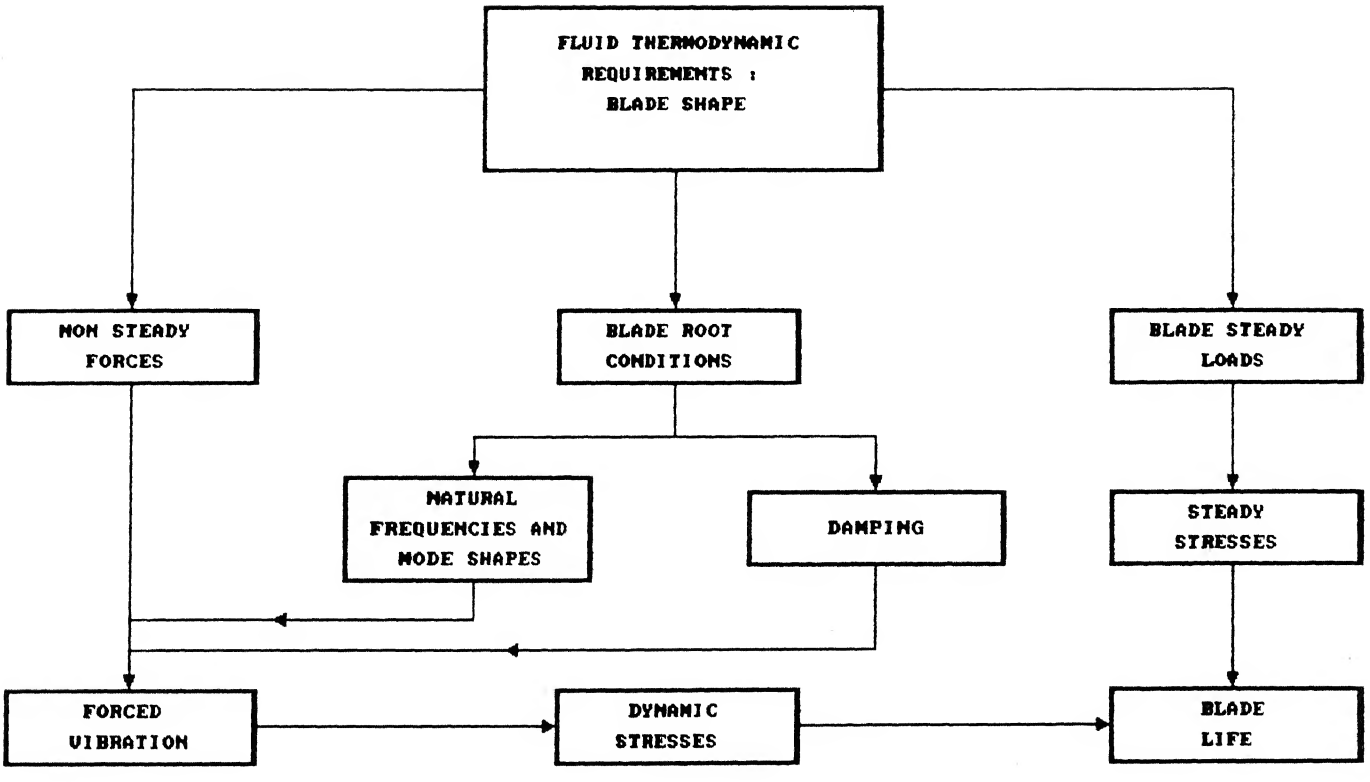

Fig. 1.1 STEPS IN THE DESIGN OF A TURBINE BLADE

The major hurdles faced in approaches to blade fatigue analyses have been [1]

- a precise evaluation of nozzle excitation forces.
- obtaining valid damping coefficients for the blade.
- determination of dynamic stresses under nonlinear damping.
- analysis of blade behaviour during transient operations like start-up and shut-down.
- definition of a failure prediction model along with evaluation of blade fatigue strength properties under broad conditions of operating environment.

1.1 PRESENT WORK

This study concerns itself with the following two aspects of blade design

- development of a numerical procedure to determine dynamic stresses under nonlinear damping. (Existing data, in literature, for typical blades has been employed for illustration).
- development of a failure prediction model based on strain-life and fracture mechanics concepts.

A software package has been developed which requires the inputs

- blade geometric and material data
- excitation data
- damping data
- operational data
- fatigue parameters

to yield outputs of

- natural frequencies and mode shapes
- dynamic stress and displacement fields under forced vibration due to nozzle excitation
- fatigue life estimate

Starbase graphics support has been used to depict the results graphically, wherever necessary.

Relevant literature has been surveyed in Chapter 2.

Chapter 3 outlines the various steps in the dynamic stress analysis of blades and describes the procedure to incorporate nonlinear damping in the analysis. Results are presented for a typical turbine blade using the data available in literature.

The fatigue life estimation model, developed on strain-life and fracture mechanics concepts, is given in Chapter 4. Implementation of the model is illustrated for assumed cases of blade defects.

Chapter 5 concludes the present work, outlining the scope for future work.

CHAPTER 2

LITERATURE REVIEW

Blade vibration has been an area of intensive research. A single free standing blade can be considered as a pre-twisted cantilever beam with an asymmetric aerofoil cross-section mounted at a stagger angle on a rotating disc. The blade executes vibrations in coupled bending-torsion modes, as the centre of flexure may not coincide with the centroid for the aerofoil cross-section and coupled bending-bending modes due to pre-twist. The problem is complicated by other effects such as shear deflections, rotary inertia, warping of the cross-section, root fixing and Coriolis acceleration. Various researchers have derived solutions to the problem by considering individual aspects such as taper, pre-twist, asymmetry of cross-section and centrifugal forces, and have made simplified assumptions towards secondary effects. They have used two distinct approaches towards blade vibration problem :

- Continuum model approach
- Discrete model approach

In the first approach, the energy terms are set up using the beam or plate theory (depending on the aspect ratio) and the solutions to the equations of motion are obtained directly by energy methods like Rayleigh-Ritz, Galerkin, Lagrange, Reissner and

Nemat-Nassar based on the Hamilton's principle. Other methods of solving differential equations of motion of cantilever blades are Integral equation approach, Perturbation and Collocation procedures. The literature in this area has been reviewed by Rao [2] and reference can be made to this paper for a detailed description of the contribution made by various researchers.

Discrete model approaches like Finite Difference Method and Finite Element Method are adopted by some researchers. Finite Difference Method has been adopted by Carnegie et al [3, 4] for rotating asymmetric blades. Sisto and Chang [5] have adopted the finite element method for rotating beam type blades. Rawtani and Dokainish [6] used FEM to determine natural modes of pre-twisted cantilever plates. Bossack and Zienkiewicz [7] extended this to rotating blades. Leissa, Macbain and Kielb [8] have made a comprehensive study of the numerous previous investigations on free vibrations of pre-twisted cantilever plates.

Blade damping is a complex problem and the main damping mechanisms known to influence damping are

(1) internal friction damping at the root

(2) material hysteresis damping

(3) steam/gas dynamic damping.

The superposition of these mechanisms determines the stress levels expected in resonant vibration and establishes the susceptibility of the blade for fatigue failure.

The possible contributions from these mechanisms can be infinitely variable and no predictive theory presently exists to relate these

damping mechanisms to predict the specific blade damping parameters. Lazan [9] has given a comprehensive coverage of material damping. Hammons [10] has considered damping arising out of oscillator motion of blade in steam environment. Rieger and Beck [11] have developed a rig to simulate centrifugal forces by thermal means in order to determine effects of rotation on damping in blades. Rao, Gupta and Vyas [12] designed and built a spin rig with nozzle passing excitation simulated by electromagnets. They obtained damping ratio as a function of rotational speed and tip displacements for the first four modes. Rao and Vyas [13] subsequently developed modal damping envelopes for different critical speeds as a function of tip displacement.

The area of forced vibrations has been researched into much less when compared to free vibration analysis. Rieger and Nowak [14] have used ANSYS program to determine dynamic stresses of a blade group due to flow path excitation. Hoyniak and Fleeter [15] made an energy balance between unsteady and aerodynamic work and energy dissipated due to aerodynamic damping to predict blade resonant vibrations. contribution by some researchers in this area.

Blade fatigue is a problem currently undergoing investigations. Rieger [16] has outlined various aspects involved in undertaking life analysis of turbomachine blading. Rao and Vyas [1] have used Bagci's fatigue surface and Miner's Cumulative Damage rule for a given loading history to estimate fatigue life of blades. Rieger [17] has proposed the usage of a fracture mechanics approach to determine low cycle fatigue life, employing the necessary stress results from the

FEM analysis of Rieger and Nowak [14, 18].

CHAPTER 3

S T R E S S A N A L Y S I S

The governing blade vibration equations are presented in this chapter. Reissner's dynamic functional in conjunction with the Ritz process and Modal Analysis has been employed to formulate the problem of forced vibration of the practical case of a tapered, twisted, asymmetric, aerofoil cross-section turbine blade mounted at a stagger angle on a disc rotating with constant angular velocity (Fig 3.1). These equations, as derived by Vyas [19], ignore higher order effects such as shear deflection, rotary inertia, warping and Coriolis forces. The blade profile data, excitation and damping data are taken from the case studies of Vyas [19] for the purpose of illustration.

The numerical procedure, developed during the course of the present study, to estimate blade response under nonlinear damping, is then presented. Strength of Materials formulae are employed to obtain the stress fields. Results are obtained for stresses as functions of various vibrational and operational parameters.

3.1 EQUATIONS OF MOTION

Referring to Fig. 3.1, the kinetic energy of the blade has been obtained as [19]

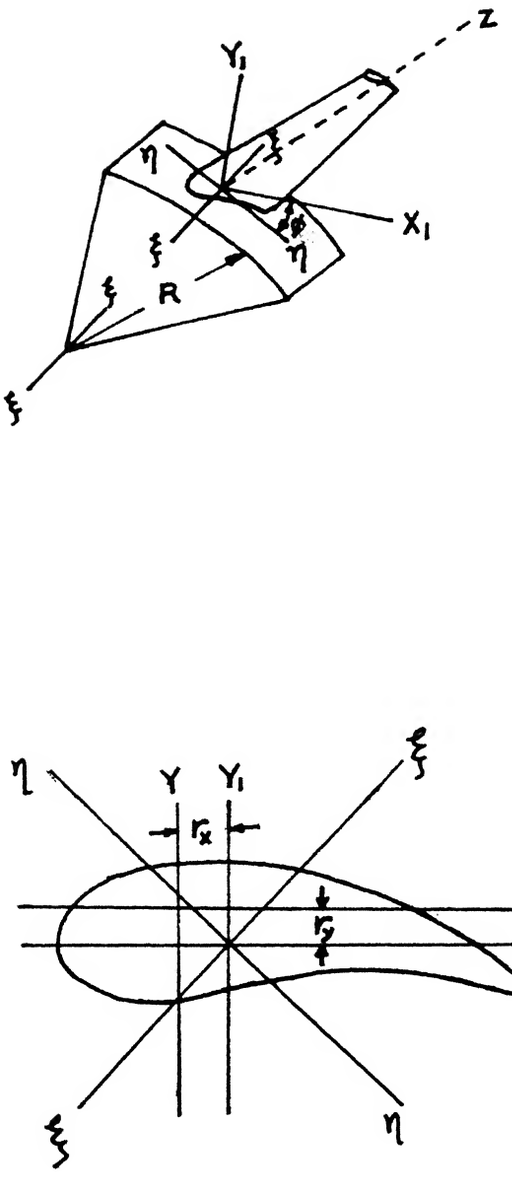

Fig. 3.1 Rotating blade with a typical cross-section

$$T = \frac{1}{2}\rho\int_0^l A\{(\dot{x} + r_y\dot{\theta})^2 + (\dot{y} - r_x\dot{\theta})^2\}\,dz + \frac{1}{2}\int_0^l I_{cg}\,\dot{\theta}^2 dz$$

$$+ \frac{1}{2}\rho\omega^2\,[-\int_0^l\{(x' + r_y\theta' + r_y'\,\theta)^2 + (y' - r_x'\,\theta - r_x\theta')^2\}(RI_1+I_2)\,dz$$

$$+ \sin^2\phi\int_0^l A(x + r_y\theta)^2\,dz + \cos^2\phi\int_0^l A(y - r_x\theta)^2\,dz$$

$$- \sin 2\phi\int_0^l A(x + r_y\theta)(y - r_x\theta)\,dz\,] \qquad (3.1)$$

where,

$$I_1 = A_0(l-z) + \frac{1}{2}A_1(l^2-z^2) + \ldots\ldots\ldots + \frac{A_n}{n+1}(l^{n+1}-z^{n+1})$$

$$I_2 = \frac{1}{2}A_0(l^2-z^2) + \frac{1}{3}A_1(l^3-z^3) + \ldots\ldots + \frac{A_n}{n+2}(l^{n+2}-z^{n+2})$$

In the equation (3.1), the first two terms represent the bending and torsional energy terms respectively while the third term is the effect of blade rotation.

The Reissner's functional is defined as [20]

$$I_R = \iiint_V \{\tau_{ij}\epsilon_{ij} - U_0^*(\tau_{ij})\}\,dv - \iiint_V B_i u_i\,dv - \iint_S T_i u_i\,ds \qquad (3.2)$$

Reissner's functional is employed in order to eliminate the shortcomings of potential energy and complementary energy methods. While potential energy methods lead to good displacement field estimates and poor stress estimates, the complementary energy methods lead to good stress estimates but poor displacement estimates. Reissner's functional yields good stress and displacement fields simultaneously since it involves both the strain and complementary energy functions.

The strain energy function for the blade is [19]

$$\int_0^l \int_A \tau_{ij}\varepsilon_{ij}\, dA\, dz = \int_0^l (-M_y x_1'' - M_x y_1'' + T_\theta \theta')\, dz \qquad (3.3)$$

The complementary energy function is

$$\iiint_V U_o^*(\tau_{ij})\, dv = \int_0^l \left[\frac{M_x^2 I_{y_1y_1} + M_y^2 I_{x_1x_1} - 2M_x M_y I_{x_1y_1}}{2E(-I_{x_1y_1}^2 + I_{x_1x_1} I_{y_1y_1})} + \frac{T_\theta^2}{2C} \right] dz \qquad (3.4)$$

The body forces are assumed to be negligible. Hence,

$$\iiint_V B_i u_i\, dv = 0 \qquad (3.5)$$

The nozzle excitation can be taken as bending forces $F_x(z,t)$ and $F_y(z,t)$ in the x and y directions and twisting moment $M(z,t)$. For a rotational frequency ω and n_s number of nozzles the excitation is periodic with nozzle passing frequency ν ($=n_s\omega$). Therefore, by Fourier expansion

$$F_x(z,t) = a_{ox}(z) + \sum_m a_{mx}(z) \cos m\nu t + \sum_m b_{mx}(z) \sin m\nu t$$

$$F_y(z,t) = a_{oy}(z) + \sum_m a_{my}(z) \cos m\nu t + \sum_m b_{my}(z) \sin m\nu t$$

$$M(z,t) = a_{oM}(z) + \sum_m a_{mM}(z) \cos m\nu t + \sum_m b_{mM}(z) \sin m\nu t \qquad (3.6)$$

The Reissner's functional is now written as

$$I_R = \int_0^l -M_y x'' - M_x y'' + T_\theta \theta' - \frac{M_x^2 I_{y_1y_1} + M_y^2 I_{x_1x_1} - 2M_x M_y I_{x_1y_1}}{2E(-I_{x_1y_1}^2 + I_{x_1x_1} I_{y_1y_1})} + \frac{T_\theta^2}{2C}\, dz$$

$$-\int_0^l \Big\{ x(z) \Big[a_{ox}(z) + \sum_m a_{mx}(z) \cos m\nu t + \sum_m b_{mx}(z) \sin m\nu t \Big] +$$

$$y(z) \Big[a_{oy}(z) + \sum_m a_{my}(z) \cos m\nu t + \sum_m b_{my}(z) \sin m\nu t \Big] +$$

$$\theta(z) \Big[a_{oM}(z) + \sum_m a_{mM}(z) \cos m\nu t + \sum_m b_{mM}(z) \sin m\nu t \Big] \Big\} dz \qquad (3.7)$$

The Reissner's dynamic functional is, therefore,

$$L = T - I_R \qquad (3.8)$$

It is to be noted that all the above expressions the cross-sectional properties like A, I etc. are taken as polynomials of z eg.

$$A(z) = A_o + A_1 z + A_2 z^2 + \ldots\ldots\ldots + A_n z^n \qquad (3.9)$$

Taking the shape functions in series form as

$$x = \sum A_i(t)\, f_i(z) \qquad M_x = \sum D_i(t)\, h_i(z)$$

$$y = \sum B_i(t)\, f_i(z) \qquad M_y = \sum E_i(t)\, h_i(z)$$

$$\theta = \sum C_i(t)\, \bar{f}_i(z) \qquad T_\theta = \sum F_i(t)\, h_i(z) \qquad (3.10)$$

where,

$$f_i(Z) = \frac{(i+2)(i+3)}{6} Z^{i+1} - \frac{i(i+3)}{3} Z^{i+2} + \frac{i(i+1)}{6} Z^{i+3}$$

$$\bar{f}_i(Z) = Z^i - \frac{i}{i+1} Z^{i+1}$$

$$h_i(Z) = (1-Z)^i/(i+1)$$

$$Z = z / l \qquad (3.10a)$$

which satisfy the boundary conditions

$$x = x' = 0 \qquad \text{and} \qquad y = y' = 0 \qquad \text{at } Z = 0$$

$$x'' = x''' = 0 \qquad \text{and} \qquad y'' = y''' = 0 \qquad \text{at } Z = 1$$

$$M_x = M_y = T_\theta = 0 \qquad \text{at } Z = 1$$

(3.11)

Applying the Ritz extremising process

$$\frac{\partial L}{\partial A_i} = \frac{\partial L}{\partial B_i} = \frac{\partial L}{\partial C_i} = \frac{\partial L}{\partial D_i} = \frac{\partial L}{\partial E_i} = \frac{\partial L}{\partial F_i} = 0 \tag{3.12}$$

the following equations of motion are obtained

$$\begin{bmatrix} M_{11} & M_{12} & \ldots & M_{1\sigma} \\ M_{21} & M_{22} & \ldots & M_{2\sigma} \\ \vdots & & & \vdots \\ M_{\sigma 1} & M_{\sigma 2} & \ldots & M_{\sigma\sigma} \end{bmatrix} \begin{Bmatrix} \ddot{A}_i \\ \ddot{B}_i \\ \vdots \\ \ddot{F}_i \end{Bmatrix} + \begin{bmatrix} K_{11} & K_{12} & \ldots & K_{1\sigma} \\ K_{21} & K_{22} & \ldots & K_{2\sigma} \\ \vdots & & & \vdots \\ K_{\sigma 1} & K_{\sigma 2} & \ldots & K_{\sigma\sigma} \end{bmatrix} \begin{Bmatrix} A_i \\ B_i \\ \vdots \\ F_i \end{Bmatrix} =$$

$$\begin{Bmatrix} Q_{01} \\ Q_{02} \\ \vdots \\ Q_{0\sigma} \end{Bmatrix} + \sum_m \begin{Bmatrix} Q_{m1} \\ Q_{m2} \\ \vdots \\ Q_{m\sigma} \end{Bmatrix} \cos m\nu t + \sum_m \begin{Bmatrix} Q_{m+\sigma,1} \\ Q_{m+\sigma,2} \\ \vdots \\ Q_{m+\sigma,\sigma} \end{Bmatrix} \sin m\nu t$$

(3.13)

where the sub-matrices

$$M_{11} = \rho \int_0^l A\, f_i f_j \, dz$$

$$M_{19} = \rho \int_0^l A\, r_y g_i f_j \, dz$$

$$M_{22} = \rho \int_0^l A\, f_i f_j \, dz$$

$$M_{29} = \rho \int_0^l A\, r_x g_i f_j \, dz$$

$$M_{91} = \rho \int_0^l A\, f_i r_y g_j \, dz$$

$$M_{32} = \rho \int_0^l A\, r_x f_i g_j \, dz$$

$$M_{33} = \int_0^l [\rho A\, (r_x^2 + r_y^2) + I_{cg}\,] g_i g_j \, dz$$

$$K_{11} = -\rho\omega^2 \left[- \int_0^l f_i' f_j' \, (RI_1 + I_2) \, dz + \sin^2\phi \int_0^l A\, f_i f_j \, dz \right]$$

$$K_{12} = \frac{1}{2} \rho\omega^2 \sin 2\phi \int_0^l A\, f_i f_j \, dz$$

$$K_{13} = -\rho\omega^2 \left[-\int_0^l \{(r_y' g_i + r_y g_i') f_j \}(RI_1 + I_2) \, dz + \right.$$

$$\left. + \sin^2\phi \int_0^l A\, r_y g_i f_j \, dz + \frac{1}{2} \sin 2\phi \int_0^l A\, r_x g_i f_j \, dz \right]$$

$$K_{15} = - \int_0^l h_i f_j'' \, dz$$

$$K_{21} = - \rho\omega^2 \sin 2\phi \int_0^l A\, f_i f_j \, dz$$

$$K_{22} = - \rho\omega^2 \left[- \int_0^l f_i' f_j' \, (RI_1 + I_2) \, dz + \cos^2\phi \int_0^l A\, f_i f_j \, dz \right]$$

$$K_{23} = -\rho\omega^2 \left[-\int_0^l \{(r_x' g_i + r_x g_i') f_j \}(RI_1 + I_2) \, dz \right.$$

$$\left. - \cos^2\phi \int_0^l A\, r_x g_i f_j \, dz + \frac{1}{2} \sin 2\phi \int_0^l A\, r_y g_i f_j \, dz \right]$$

$$K_{24} = - \int_0^l h_i f_j'' \, dz$$

$$K_{31} = -\rho\omega^2 \left[-\int_0^l \{ f_i' (r_y' g_j + r_y g_j') \}(RI_1 + I_2) \, dz \right.$$

$$\left. + \sin^2\phi \int_0^l A\, r_y g_j f_i \, dz + \frac{1}{2} \sin 2\phi \int_0^l A\, r_y g_j f_i \, dz \right]$$

$$K_{32} = -\rho\omega^2 \left[-\int_0^l \{ f_i' (r_x' g_j + r_x g_j') \}(RI_1 + I_2) \, dz \right.$$

$$\left. - \cos^2\phi \int_0^l A\, r_x g_j f_i \, dz - \frac{1}{2} \sin 2\phi \int_0^l A\, r_y g_j f_i \, dz \right]$$

$$K_{33} = -\rho\omega^2 \left[-\int_0^l \{(r_y' g_i + r_y g_i')^2 - (r_x' g_i + r_x g_i')^2 \}(RI_1 + I_2) \, dz \right.$$

$$+ \sin^2\phi \int_o^l A\, r_y^2 g_j g_j \, dz + \cos^2\phi \int_o^l A\, r_x^2 g_i g_j \, dz$$

$$+ \sin 2\phi \int_o^l A\, r_x g_i g_j \, dz \;]$$

$$K_{36} = - \int_o^l h_i g_j' \, dz$$

$$K_{42} = - \int_o^l h_j f_i'' \, dz$$

$$K_{44} = \int_o^l \frac{h_i h_j I_{y_i y_i}}{E(I^2_{x_i y_i} - I_{x_i x_i} I_{y_i y_i})} \, dz$$

$$K_{45} = - \int_o^l \frac{h_i h_j I_{y_i y_i}}{E(I^2_{x_i y_i} - I_{x_i x_i} I_{y_i y_i})} \, dz$$

$$K_{51} = K_{42}$$

$$K_{54} = K_{45}$$

$$K_{55} = \int_o^l \frac{h_i h_j I_{x_i y_i}}{E(I^2_{x_i y_i} - I_{x_i x_i} I_{y_i y_i})} \, dz$$

$$K_{63} = - \int_o^l h_j g_i' \, dz$$

$$K_{66} = - \int_o^l \frac{h_i h_j}{C} \, dz$$

$$Q_{o1} = \int_o^l a_{ox} f_j \, dz \qquad Q_{m,1} = \int_o^l a_{mx} f_j \, dz \qquad Q_{m+6,1} = \int_o^l b_{mx} f_j \, dz$$

$$Q_{o2} = \int_o^l a_{oy} f_j \, dz \qquad Q_{m,2} = \int_o^l a_{my} f_j \, dz \qquad Q_{m+6,2} = \int_o^l b_{my} f_j \, dz$$

$$Q_{o3} = \int_o^l a_{oM} g_j \, dz \qquad Q_{m,3} = \int_o^l a_{mM} g_j \, dz \qquad Q_{m+6,3} = \int_o^l b_{mx} g_j \, dz$$

(3.14)

All other elements are zero.

3.2 DAMPING

In the present study blade damping is modelled as a nonlinear function of strain amplitude and speed of rotation for each mode of vibration. For ease of formulation, initially, damping is assumed to be viscous and proportional so that the energy dissipated is

$$W_d = C_v \, T \, / \, \rho \tag{3.15}$$

The process of incorporating the nonlinear damping is considered later, in section 3.4.

The equations of motion for forced damped vibration are

$$[M]\{\ddot{q}\} + [C]\{\dot{q}\} + [K]\{q\} = \{Q_o\} + \sum_m \{Q_m\} \cos m\nu t + \sum_m \{Q_{m+\sigma}\} \sin m\nu t \tag{3.16}$$

where

$$\{q\}^T = \{ A_i, \ldots . D_i, .. F_i \}$$

The damping submatrices are

$$C_{11} = \frac{C_v}{\rho} M_{11}$$

$$C_{12} = \frac{C_v}{\rho} M_{12} \quad \text{etc.} \tag{3.17}$$

The rest of the elements are as given by equations (3.14).

3.3 MODAL ANALYSIS

Modal analysis is used to obtain the decoupled equations of forced motion. Using

$$\{q\} = [U] \{\eta\} \tag{3.18}$$

the decoupled equations of motion are

$$[\bar{M}]\{\ddot{\eta}\} + [\bar{C}]\{\dot{\eta}\} + [\bar{K}]\{\eta\} = \{Q_{oN}\} + \sum_m \{Q_{mN}\} \cos m\nu t + \sum_m \{Q_{(m+\sigma)N}\} \sin m\nu t \qquad (3.19)$$

where

$$[\bar{M}] = [U]^T [M] [U]$$

$$[\bar{C}] = [U]^T [C] [U]$$

$$[\bar{K}] = [U]^T [K] [U]$$

and

$$\{Q_{oN}\} = [U]^T \{Q_o\}$$

$$\{Q_{mN}\} = [U]^T \{Q_m\}$$

$$\{Q_{(m+\sigma)N}\} = [U]^T \{Q_{m+\sigma}\}$$

The individual uncoupled equations are of the form

$$M_k(\ddot{\eta}_k + 2\zeta_k p_k \dot{\eta}_k + p_k^2 \eta_k) = Q_{oN_k} + \sum_m Q_{mN_k} \cos m\nu t + \sum_m Q_{(m+\sigma)N_k} \sin m\nu t \qquad (3.20)$$

where

$$p_k^2 = K_k / M_k$$

$$\zeta_k = C_k / 2M_k p_k$$

for which the solution due to each term in the forcing function is written as

$$\eta_{o_k} = \frac{Q_{oN_k} / M_k}{p_k^2}$$

$$\eta_{m_k} = \frac{Q_{mN_k} / M_k}{\sqrt{[p_k^2 - (m\nu)^2]^2 + 4\zeta_k^2 p_k^2 (m\nu)^2}} \cos(m\nu t - \psi_{m_k})$$

$$\eta_{(m+\sigma)_k} = \frac{Q_{(m+\sigma)N_k} / M_k}{\sqrt{[p_k^2 - (m\nu)^2]^2 + 4\zeta_k^2 p_k^2 (m\nu)^2}} \sin(m\nu t - \psi_{m_k}) \tag{3.21}$$

where

$$\psi_{m_k} = \tan^{-1} \frac{2\zeta_k p_k (m\nu)}{p_k^2 - (m\nu)^2}$$

The response due to each harmonic can be written as

$$H_{o_k} = \eta_{o_k} = \frac{Q_{oN_k} / M_k}{p_k^2}$$

$$H_{m_k} = \eta_{m_k} + \eta_{(m+\sigma)_k}$$

$$= \frac{\sqrt{Q_{mN_k}^2 + Q_{(m+\sigma)N_k}^2} / M_k}{\sqrt{[p_k^2 - (m\nu)^2]^2 + 4\zeta_k^2 p_k^2 (m\nu)^2}} \cos(m\nu t - \psi_{m_k} - \delta_{m_k}) \tag{3.22}$$

where

$$\delta_{m_k} = \tan^{-1} \frac{Q_{(m+\sigma N_k}}{Q_{mN_k}}$$

The following formulae are used for the computation of stresses

$$M_X = M_x \cos\phi_z - M_y \sin\phi_z$$

$$M_Y = M_y \cos\phi_z + M_x \sin\phi_z$$

The normal stress is

$$\sigma_z = \frac{M_Y X}{I_{yy}} + \frac{M_X Y}{I_{xx}}$$

The maximum shear stress occurs in the vicinity of one of the points where the largest inscribed circle touches the boundary of the

blade profile of the section [21]. This stress is given by

$$\tau_{r\theta} = \frac{T_\theta}{K} C$$

where

$$K = \frac{\frac{1}{3} F}{1 + \frac{4}{3} F/AU^2} \quad ; \quad F = \int_0^l t^3 \, du$$

in which

du = elemental length along the camber line

t = profile thickness as a function of u

A = area of the section

$$C = \frac{D}{1 + \frac{\pi^2 D^4}{16A^2}} \left[1 + 0.15 \left(\frac{\pi^2 D^4}{16A^2} - \frac{D}{2r} \right) \right]$$

if the radius of curvature of the profile at the point is positive

$$C = \frac{D}{1 + \frac{\pi^2 D^4}{16A^2}} \left[1 + \left(0.118 \, ln \left(1 - \frac{D}{2r} \right) - 0.238 \frac{D}{2r} \right) \tan \frac{2\phi}{\pi} \right]$$

if the radius of curvature of the profile at the point is negative

D = diameter of the inscribed circle

r = radius of curvature of the profile at the point

ϕ = angle through which a tangent to the boundary rotates in turning or travelling around the reentrant position (radians)

Stresses τ_{zx} and τ_{yz} are obtained from $\tau_{r\theta}$ using coordinate

transformation relations.

The principal stresses are

$$\sigma_1 = 0$$

$$\sigma_{2,3} = \frac{\sigma_z}{2} \pm \sqrt{\left(\frac{\sigma_z}{2}\right)^2 + \tau_{zx}^2 + \tau_{yz}^2} \qquad (3.23)$$

The basic mean stress (zeroth harmonic) and alternating stresses are determined from the principal stresses by using the formula

$$\sigma_m \ , \quad \sigma_{alt} = \sqrt{\left[\sigma_2^2 + \sigma_3^2 - \sigma_2\sigma_3\right]} \qquad (3.24)$$

3.4 DAMPING MODEL

Damping is a critical parameter in the stress analysis of turbomachinery blading. It determines the stress levels expected in resonant vibrations. The main damping mechanisms influencing blade behaviour are interfacial damping at the root, material damping and gas / steam damping.

Rao, Gupta and Vyas [12] conducted tests in vacuum spin rig and established the dependency of overall damping on the rotational speed and strain amplitude. In these tests, excitation was provided by electromagnets simulating nozzles in a turbomachine. From the filtered decay signals of each mode, equivalent modal damping ratios were obtained as function of rotational speed and strain amplitude. Typical equivalent modal damping values for the first mode obtained experimentally by Vyas [19] are shown in Fig.3.8.

The earlier study by Vyas [19], however averaged the modal damping value over the range of vibration amplitude (for the speed under consideration). He assumed that this average can be taken as a constant damping value which is valid for all amplitudes and employed it for the purpose of stress analysis. In the present study, an improvement has been made over the above approach by making a provision for the amplitude dependence of damping. The damping ratios for each mode can be expressed as polynomial functions of strain amplitude, ϵ , at various rotor speeds. Thus,

$$\zeta = a_0 + a_1 \epsilon + a_2 \epsilon^2 + \ldots\ldots + a_5 \epsilon^5 \qquad (3.25)$$

The constants a_i in the above equation can be obtained by a curve fitting routine. The strain amplitude, ϵ, is however, itself determined by the damping, ζ. Hence, an iterative procedure is adopted.

Starting with an assumed value of strain and corresponding modal damping ratio, point 1, Fig. 3.2, the principal component of stress and resultant strain is estimated, point 1'. The average of the assumed and estimated values of strain and the corresponding modal damping ratio are taken as the starting values for the next iteration. The process is repeated till two successive values of stress are obtained within a specified level of accuracy.

3.5 COMPUTER PROGRAM

The computer program developed for studying the blade vibration is modular in form. Individual modules can be attached or removed

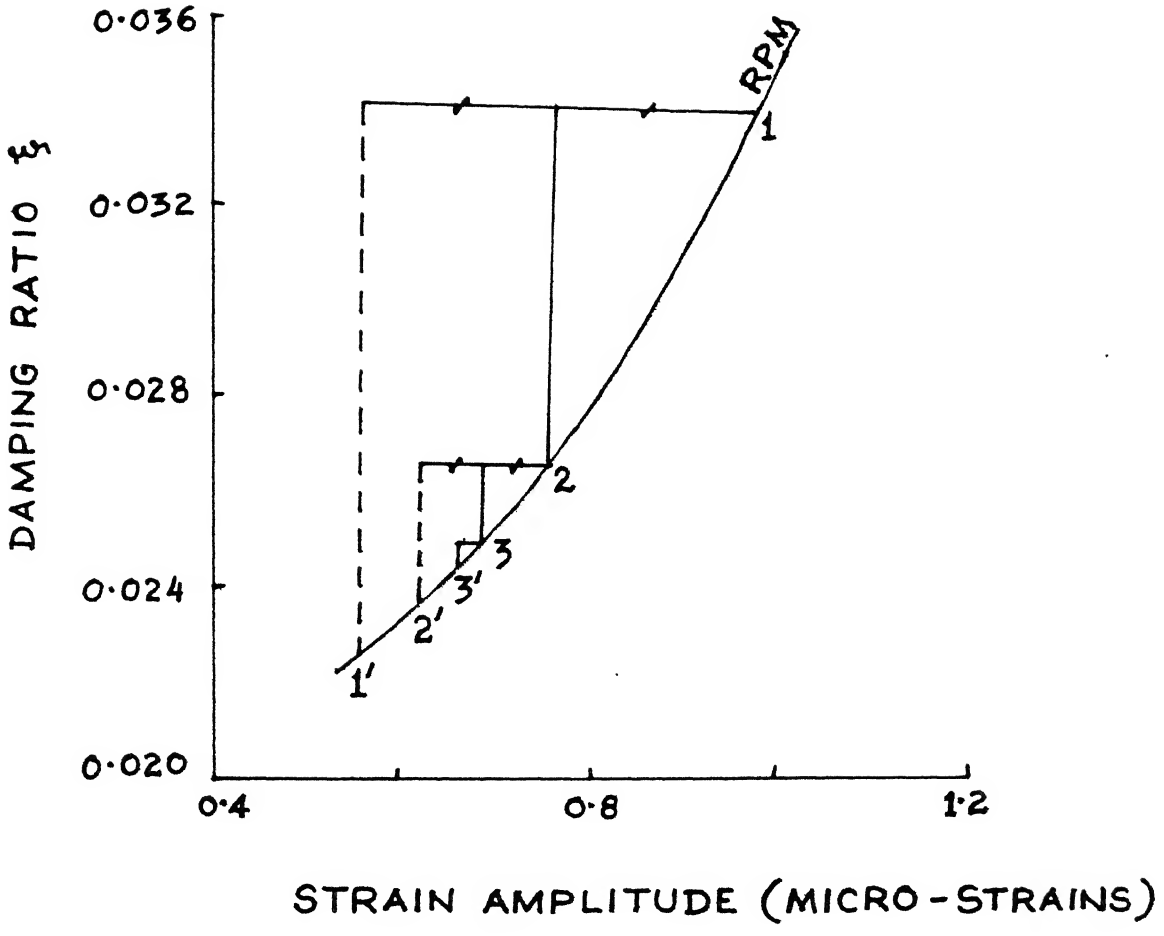

Fig. 3.2 Iteration procedure

depending on the requirement. Each module can be run independently and in tandem with the main program. Starbase graphics library support has been taken to present the result in a graphical form for easier interpretation. Fig. 3.3 gives the structure of the software developed. It is briefly outlined below.

The package requires the following inputs to be fed by the user:

1. Blade sectional profile data ——→ sect.dat
2. Blade material properties ——→ mat.dat
3. Blade damping data ——→ damp_pl.dat
4. Nozzle excitation data ——→ excit.dat

flex.f — reads data from sect.dat and computes the coordinates of the centre of flexure of the aerofoil cross-section.

sect.f — reads data from sect.dat and flex.out and determines the area, second area moments of the cross-section about x and y axis, product moment of cross-section about x-y axis, polar moment of inertia about an axis passing through the centre of flexure and the torsional stiffness of the cross-section.

damp.f — reads standard values of damping ratio from damp_pl.dat and computes the damping curves for the particular speed at which the rotor is being run. It first locates that particular speed between two speeds for which damping data is known. It then

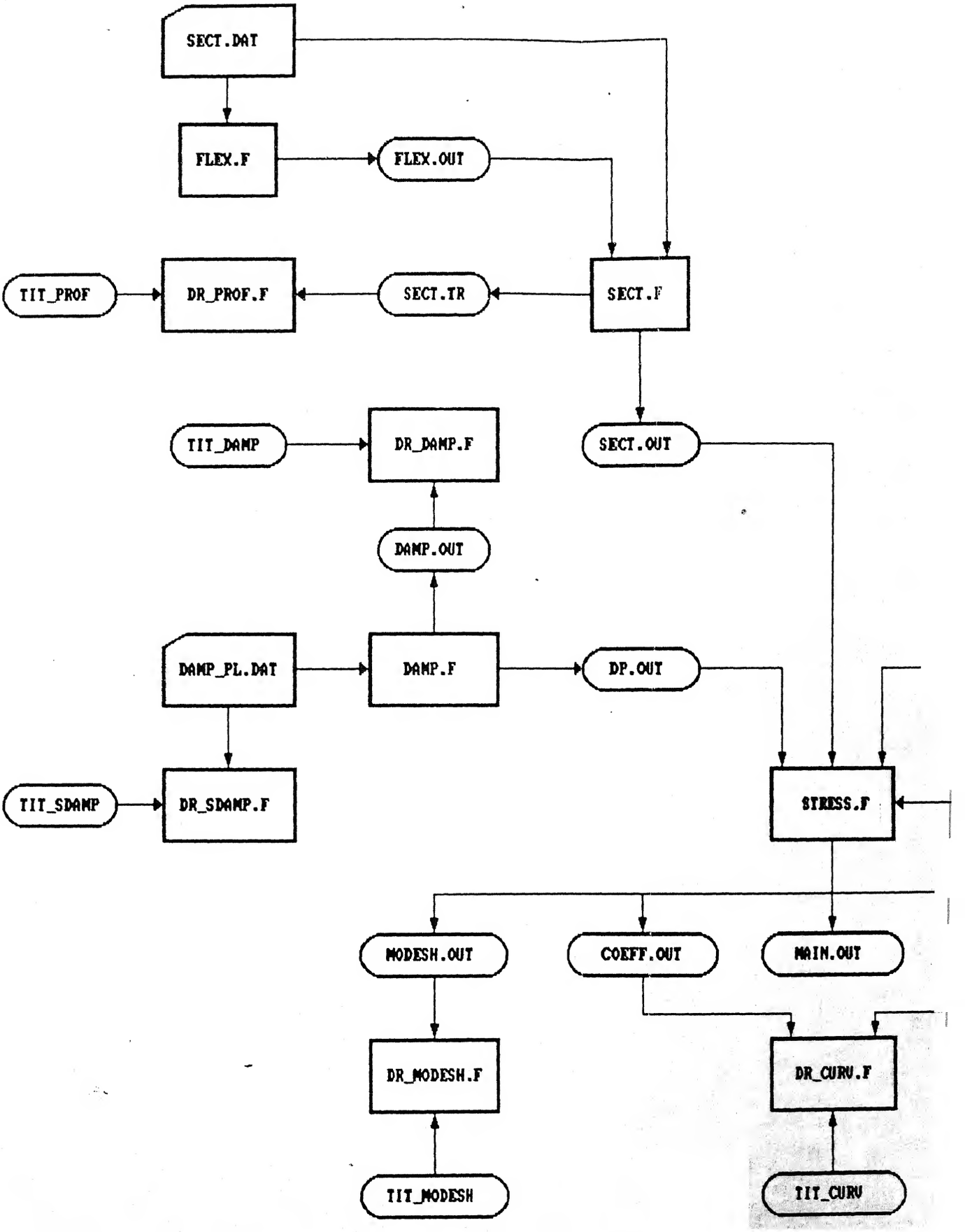

FIG. 3.3 SOFTWARE

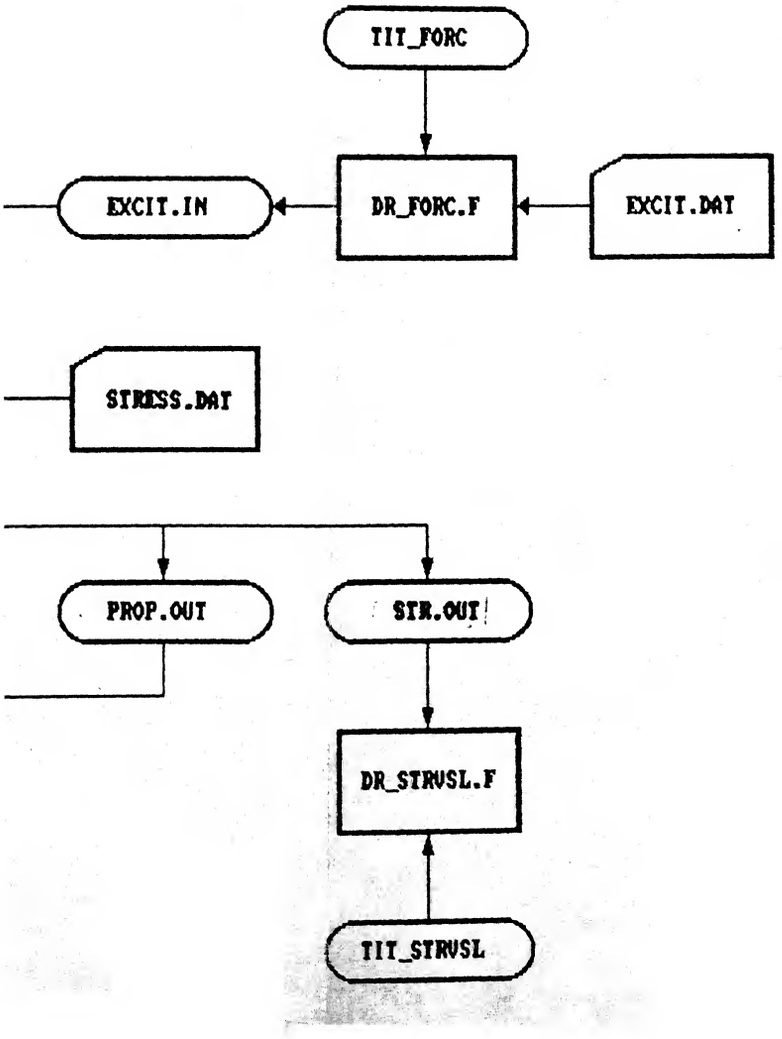
TIT_FORC
EXCIT.IN
DR_FORC.F
EXCIT.DAT
STRESS.DAT
PROP.OUT
STR.OUT
DR_STRUSL.F
TIT_STRUSL

STRUCTURE

interpolates the damping values and obtains the damping curve.

dr_forc.f — reads excitation data from excit.dat and computes the Fourier force components of the forces and also plots them along with the forces.

stress.f — reads input from four files already generated, namely

a) Section properties data from sect.out
b) Excitation Fourier components from excit.in
c) Damping data for the rotor speed from dp.out
d) Material property data from stress.dat

The computation proceeds along the following lines :

1. Curve fits for the section properties with length is obtained.

2. The mass and stiffness matrices are then generated using standard quadrature formulae.

3. The eigenvalue matrix is then formulated.

4. The eigenvalue matrix is solved and eigenvalues and eigenvectors determined.

5. The natural frequencies and mode shapes are obtained using eigenvalues, eigenvectors and shape functions.

6. The generalised stiffness, mass and force matrices are obtained.

7. The decoupled equations of motion are then solved to obtain the response using any one value for the damping ratio (the maximum in this implementation).

8. The displacements are then determined and stresses obtained. The principal stresses are used to compute the strains, from which a new damping value is obtained (since strain amplitudes and damping ratio are related nonlinearly). If the old

and the new values of the damping ratios differ by a defined small quantity, then that is the correct value of damping and the stresses are reported. If they do not coincide, the average of the new and old values of the damping ratio is used and this step is again repeated.

The files with the extension dr_ are essentially graphics generating program files. Those with extension tit_ are title files and contain the text to supplement the graphics.

dr_prof.f	reads profile data arranged in a particular format from sect.tr and generates the blade profiles for various sections along the length.
dr_sdamp.f	reads standard damping data fed into damp_pl.dat and draws the standard damping data for each of the first four modes as a function of the rotor speeds.
dr_damp.f	reads data about the damping curves for the particular speed at which the rotor is being run from damp.out and draws the damping curves.
dr_modesh.f	reads data from modesh.out and draws the mode shapes.
dr_curv.f	reads data from coeff.out and prop.out and plots the various section properties, mentioned earlier, as a function of blade length.
dr_strvsl.f	reads data from str.out and draws the stresses as function of blade length for the various harmonics.
tit_prof	contains text for the drawing file dr_prof.f. Other title files operate similarly.

All the above programs are run by the file "start" which contains the commands for compiling and executing all the programs sequentially. Individual programs can be compiled individually and executed. New modules can also be added and/or deleted which is an important feature of the package.

3.6 RESULTS AND DISCUSSION

The package developed is run for an illustrative case for which data is taken from [19]. Fig.3.4 shows the six cross-sectional profiles of a typical turbine blade at different distances from the root. The various geometric properties obtained from the profiles are plotted against blade length in Figs 3.5a and 3.5b. Typical nozzle excitation forces are periodic in nature, and as simulated experimentally by means of electromagnets [19], are shown in Fig. 3.6. The same figure also shows the Fourier component amplitudes of the forcing functions. It may be noted here that the magnitudes of the excitation forces are very small since they have been obtained from laboratory simulation by electromagnets. In practice, these forces are considerably large to drive the machine for power generation. The natural frequencies are listed in Table 3.1. The mode shapes are plotted in Figs. 3.7a through 3.7e. The first and second modes are predominantly flapwise bending modes, with the twist being extremely small. The third mode shows an increasing contribution due to twist. The fourth mode is predominantly torsional. The fifth mode is a coupled mode with deflection in the bending mode dominating. Figs. 3.8 through 3.11 show the damping curves for the first four

modes at different rotor speeds. Fig. 3.12 is the Campbell diagram for the blade with six nozzle passing harmonics interacting with the natural modes to give resonant rotor speeds upto 4000 rpm. The resonant speeds are listed in Table 3.2. Figs. 3.13 through 3.15 show the damping curves for the rotor speeds at which the fourth, fifth and sixth nozzle passing frequencies interact with the first mode. The blade stress fields have been computed for various rotor speeds upto 1200 rpm including resonances. The stresses are determined at six equidistant stations along the blade length. Fig. 3.16 shows the variation of the stress harmonics at the blade root as a function of the rotor speed. Figs. 3.17a and 3.17b depict the resonant stresses as a function of blade length.

It can be observed that the stress fields on the blade are functions of the order of the nozzle passing harmonic, the amplitude of the forcing function components, the interacting blade natural mode and the blade geometry. For the resonant speed under consideration, ie. 930 rpm, the stresses are maximum at the root and decrease towards the tip. The maximum stress due to the interaction of the sixth harmonic with the first mode is greater than the corresponding value due to the interaction of the fifth harmonic with the first mode. This is because the Fourier amplitude of the fifth order harmonic is less than the sixth. A more rigorous parametric study can be undertaken, with the help of the computer package developed, for a detailed investigation of the operational and geometric parametric influences on the blade stresses.

3.7 CLOSURE

In this chapter, the dynamic stress analysis of a tapered, twisted, asymmetrical aerofoil cross-section blade has been undertaken and the computer program developed illustrated for a typical blade under forced excitation and nonlinear damping.

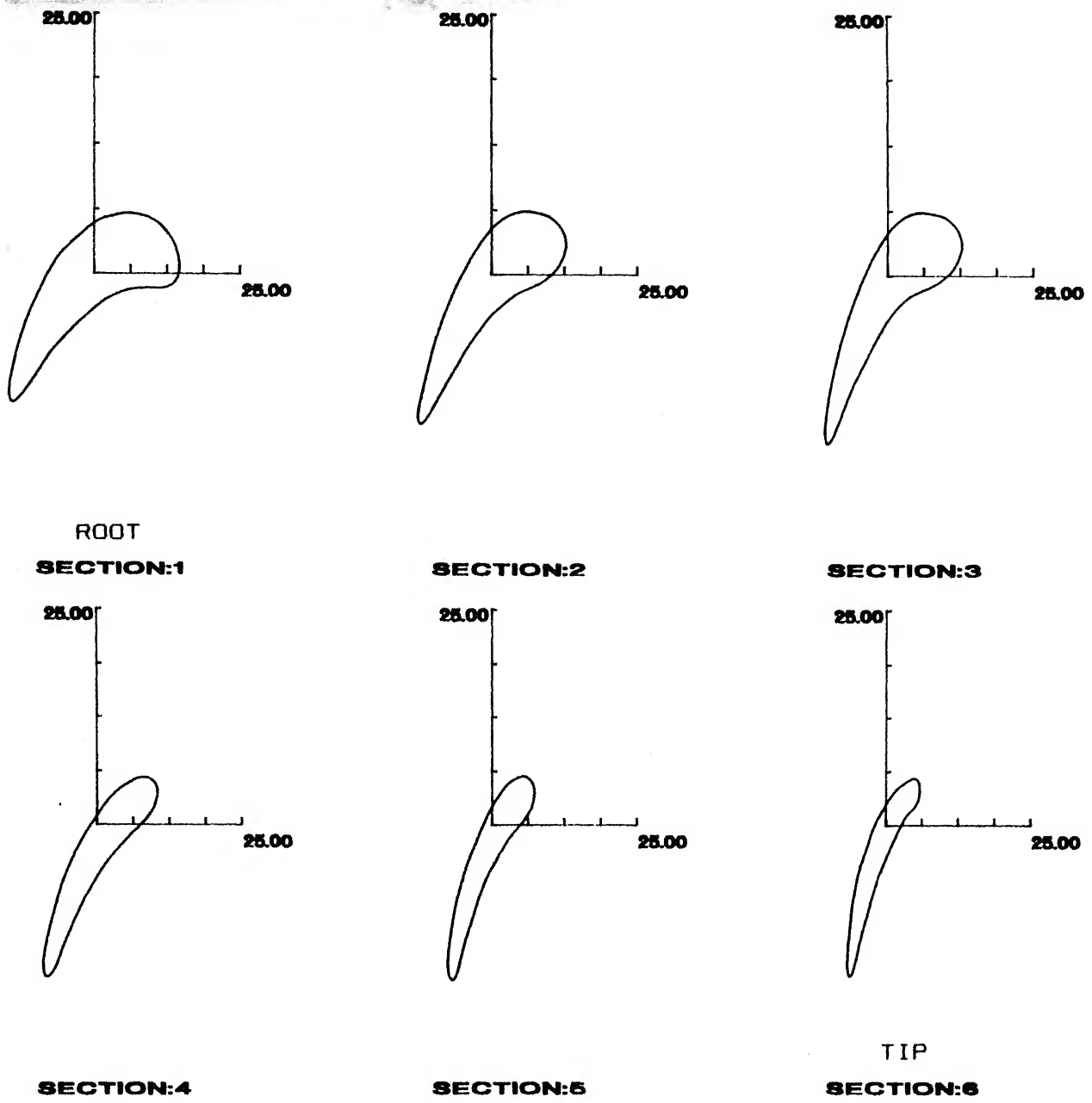

Fig. 3.4 Blade sections at various locations along its length

(Dimensions in millimeters)

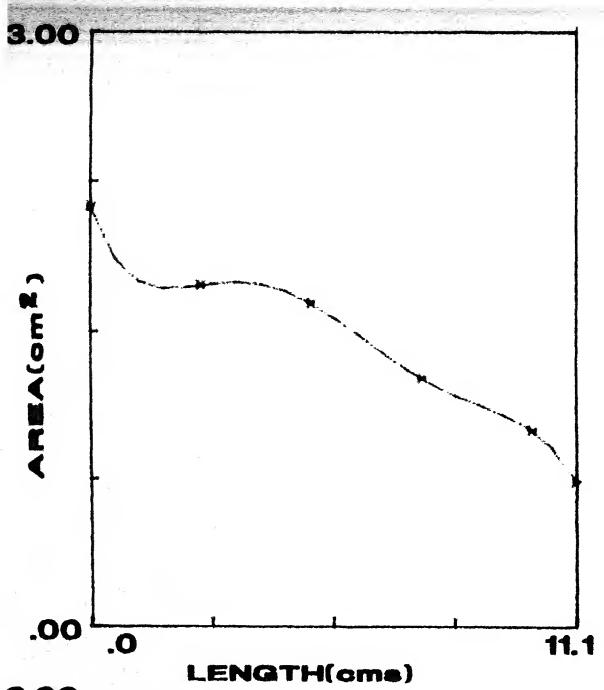

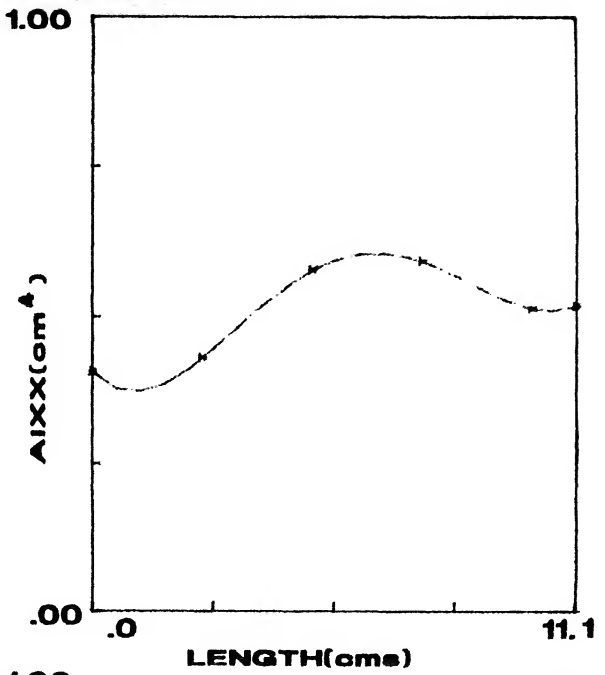

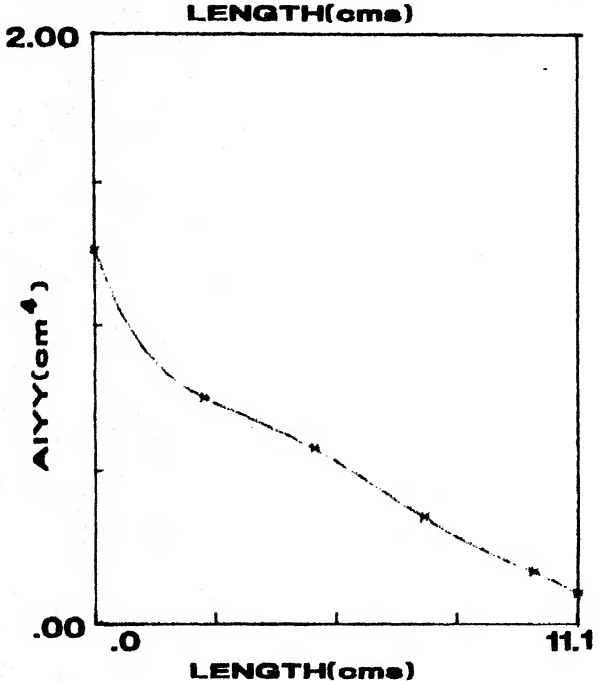

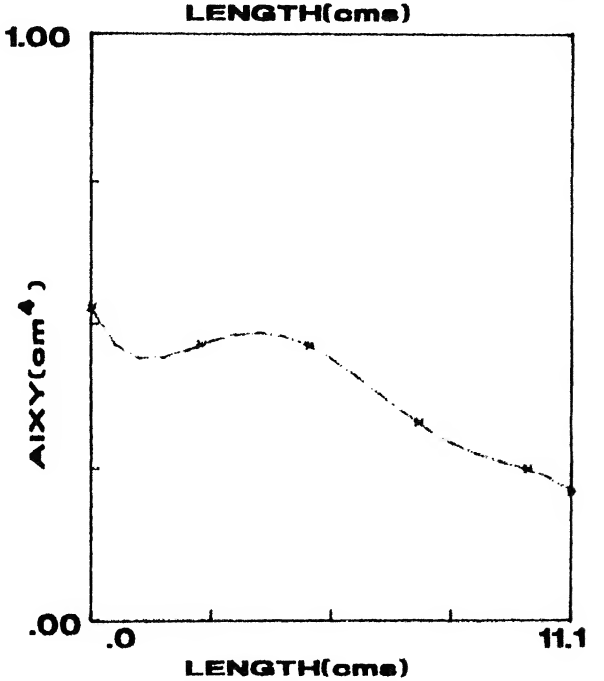

Legend

AIXX - Area Moment of Inertia about x-x

AIYY - Area Moment of Inertia about y-y

AIXY - Product Moment of Inertia

Fig. 3.5a Variation of geometrical properties with length

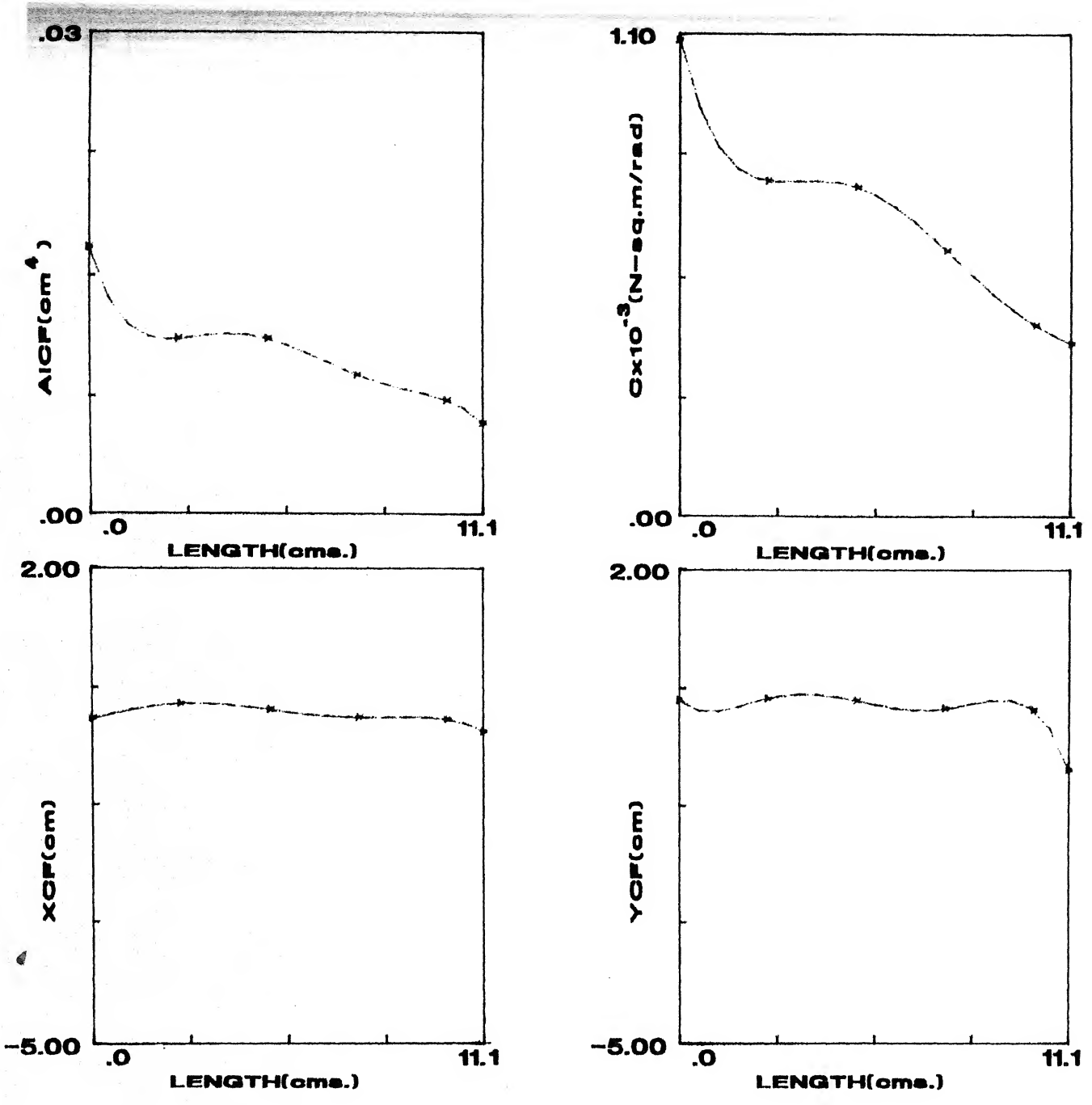

Legend

AICF - Moment of Inertia about centre of flexure

C - Torsional Stiffness

XCF, YCF - Coordinates of centre of flexurefrom c.g.

Fig. 3.5b Variation of geometrical properties with length

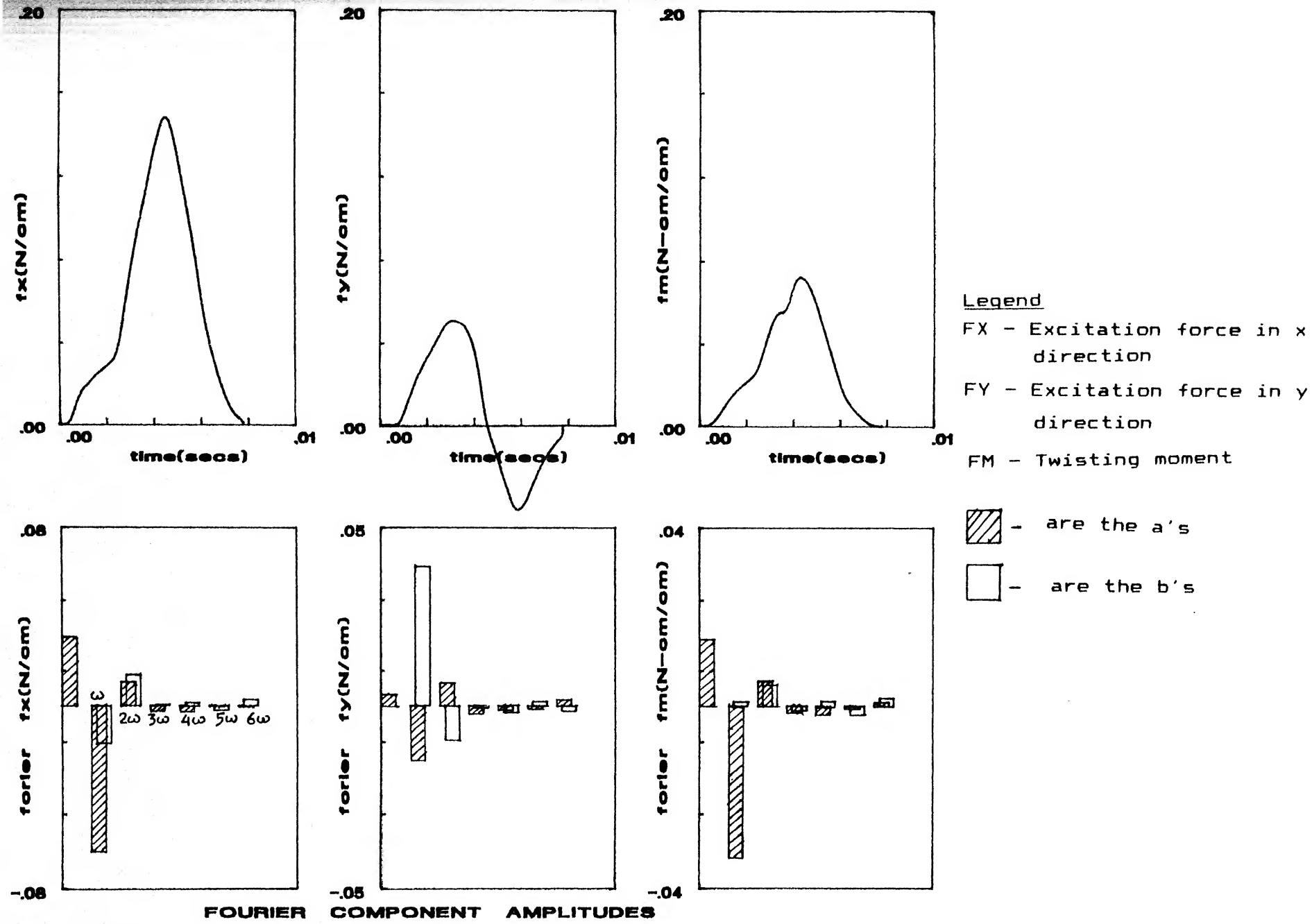

Fig. 3.6 Forcing functions and Fourier component amplitudes

TABLE 3.1

NATURAL FREQUENCIES (Hz)

1. 743.2
2. 2146.5
3. 4548.9
4. 7537.3
5. 9743.2
6. 13683.0
7. 14475.0
8. 20884.0
9. 36682.0
10. 37486.0

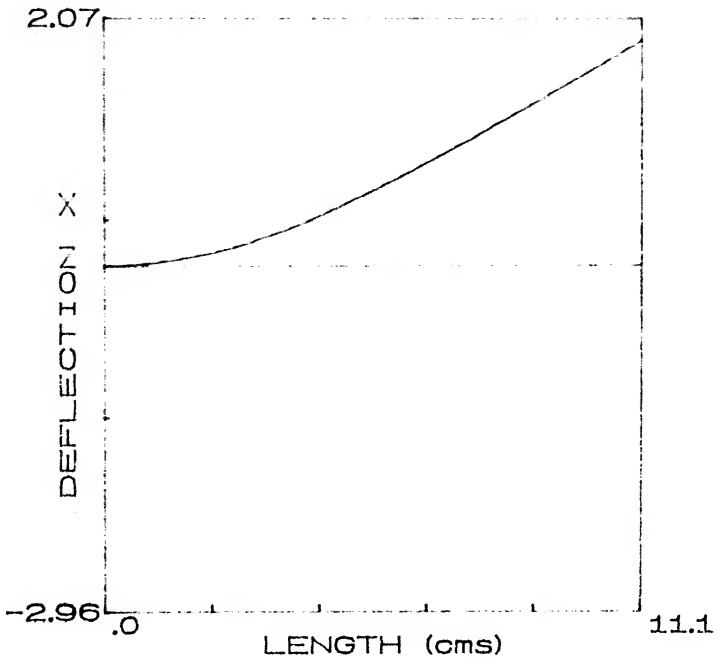

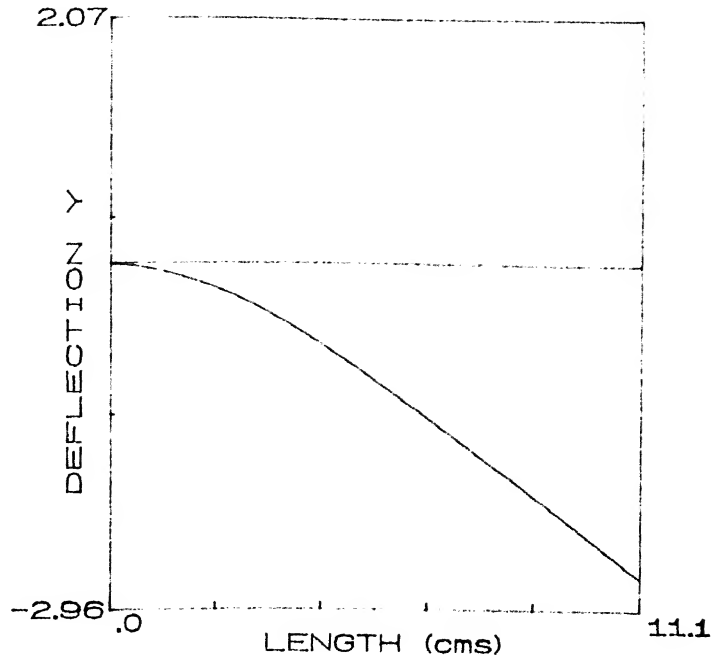

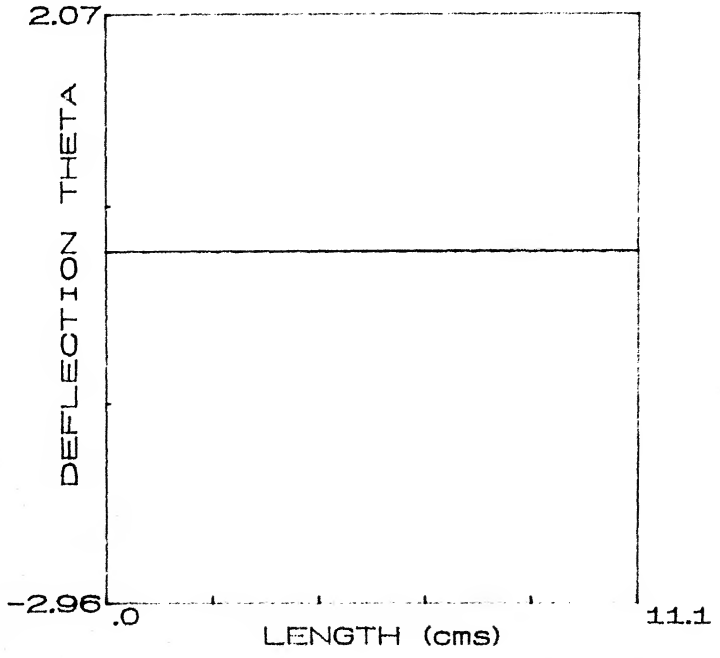

MODE # 1

NATURAL FREQUENCY (Hz): .74357E+03

Fig. 3.7a Mode shapes

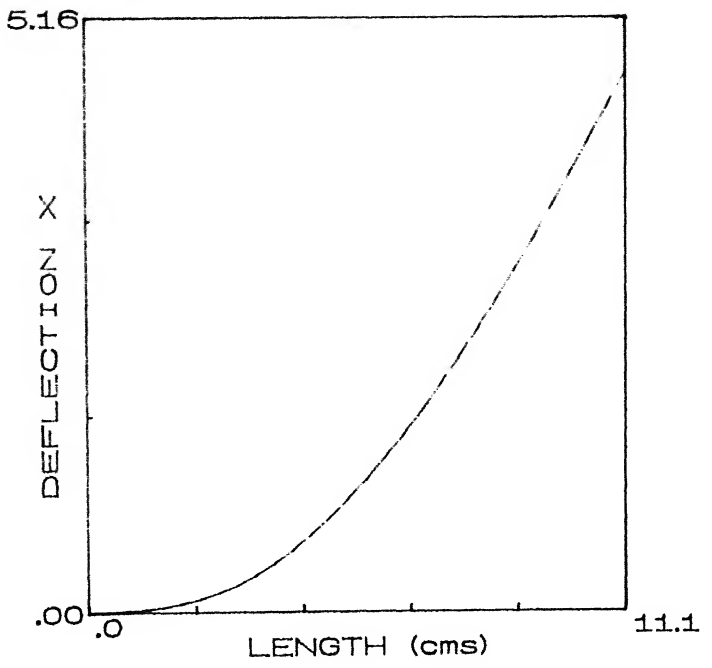

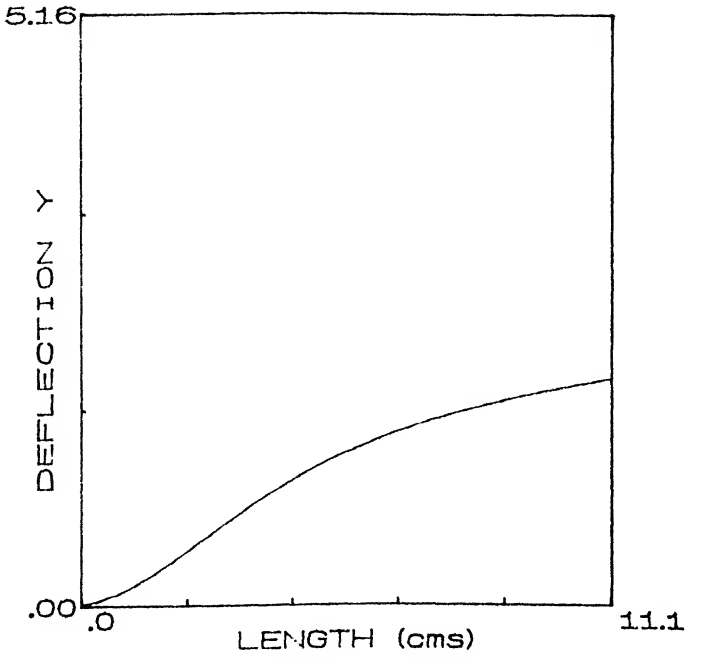

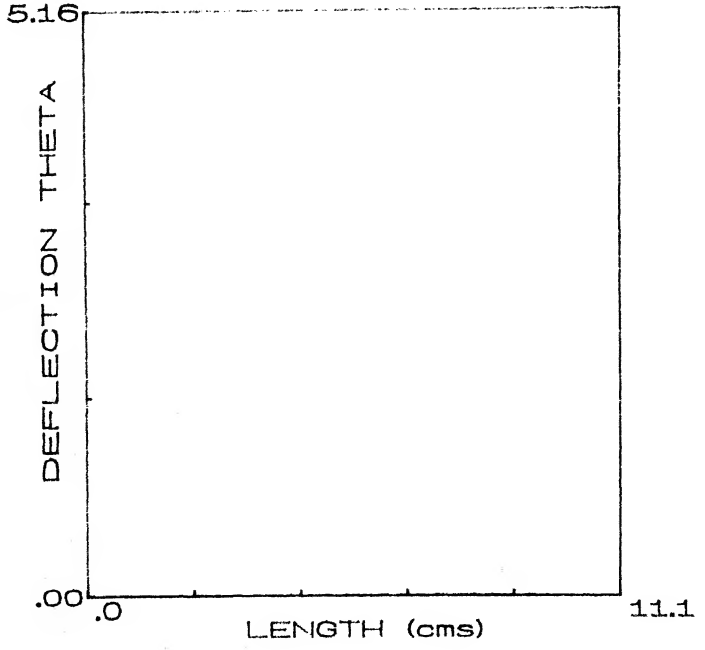

MODE # 2

NATURAL FREQUENCY (Hz): .21467E+04

Fig. 3.7b Mode shapes

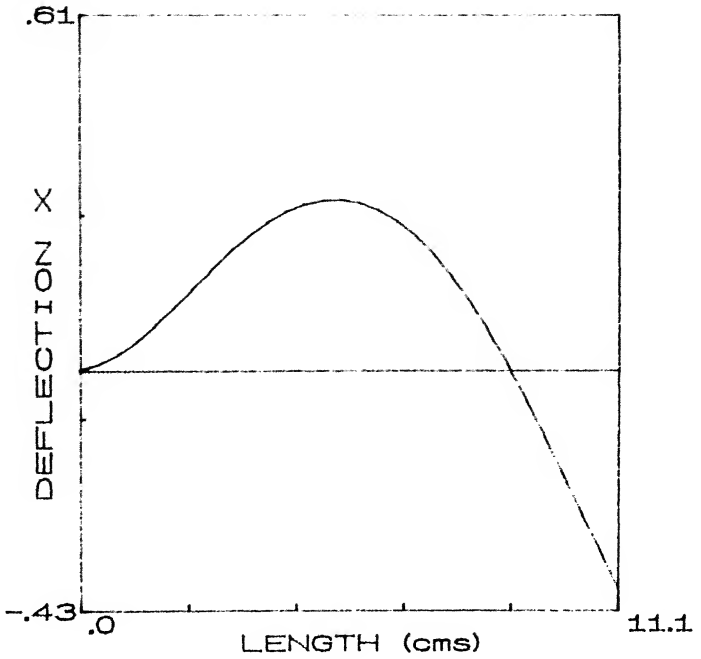

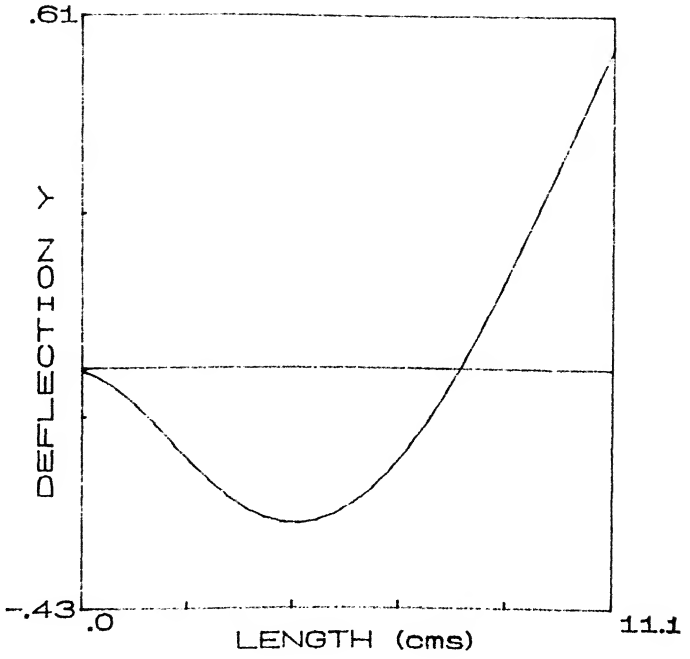

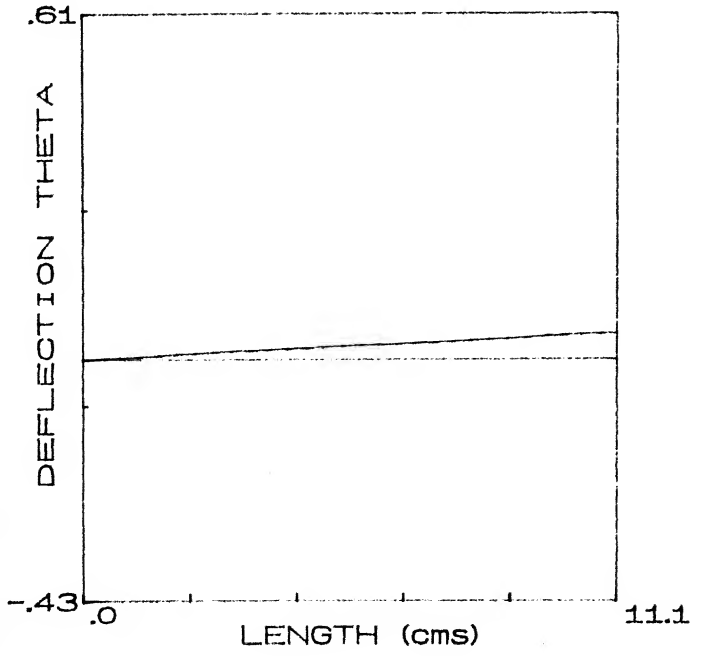

MODE # 3

NATURAL FREQUENCY (Hz): .45490E+04

Fig. 3.7c Mode shapes

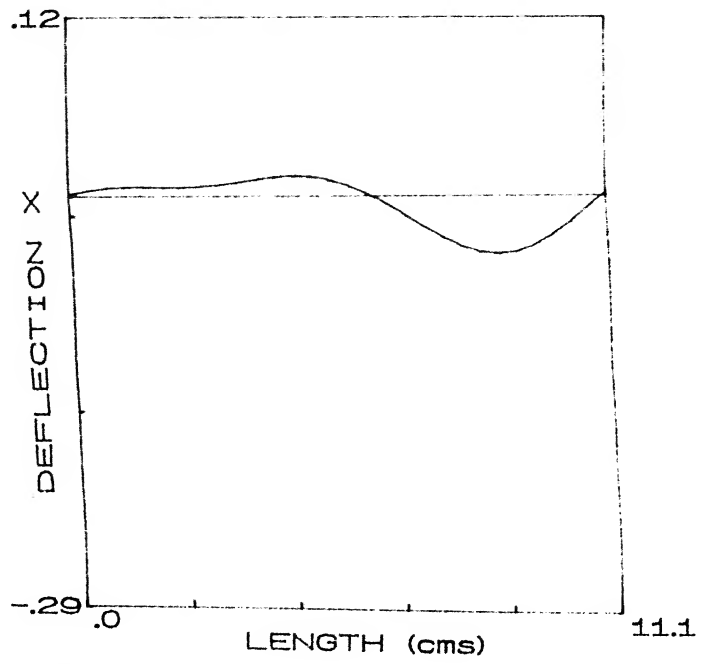

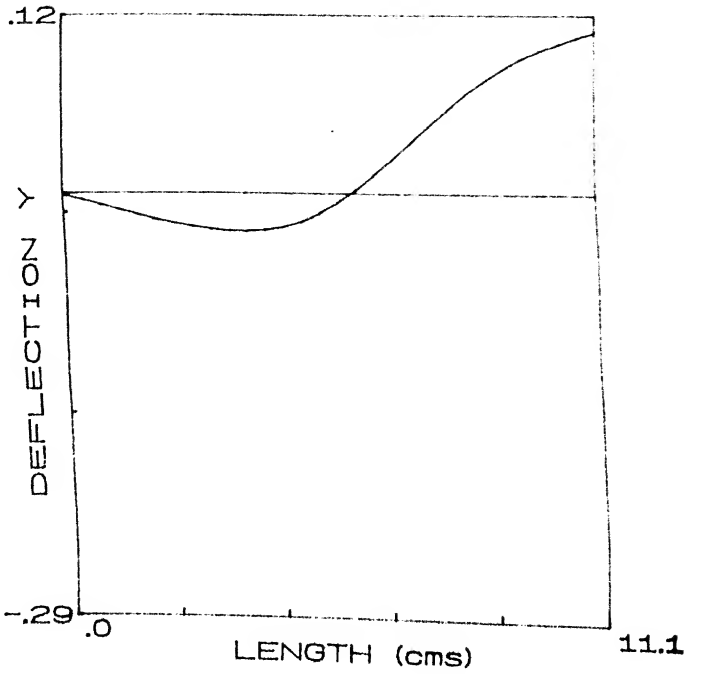

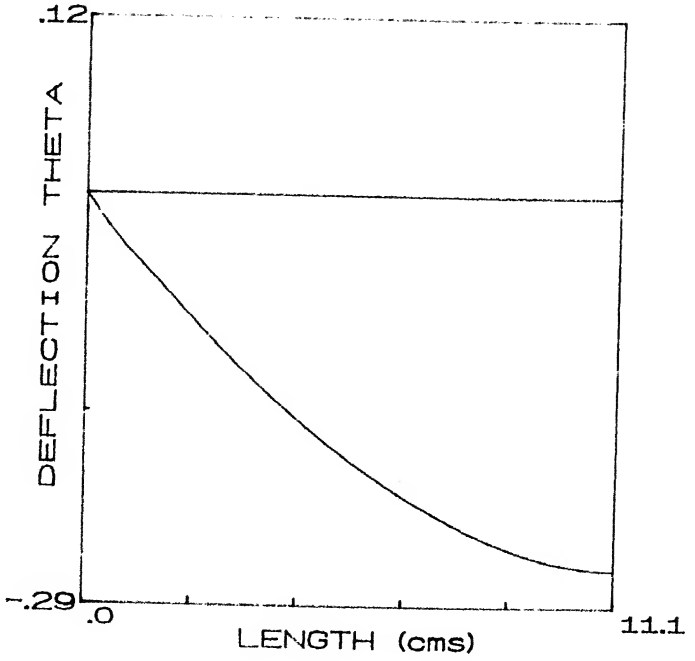

MODE # 4

NATURAL FREQUENCY (Hz): .75391E+04

Fig. 3.7d Mode shapes

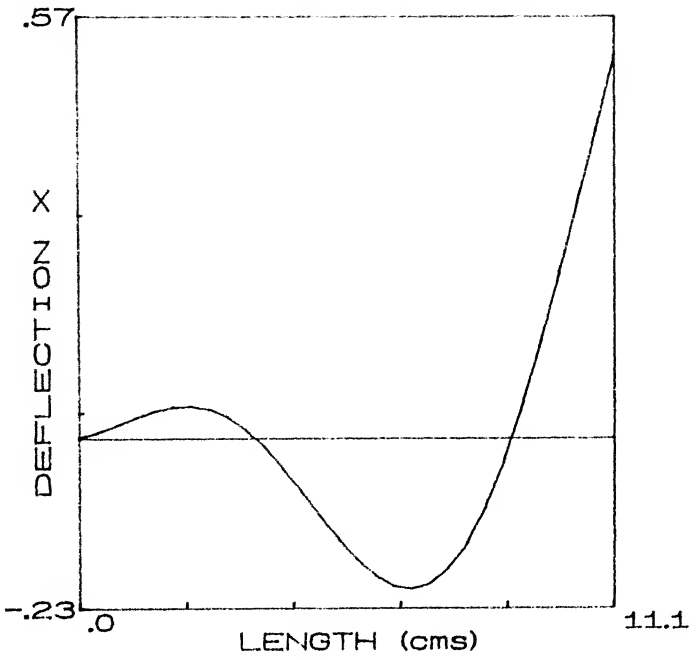

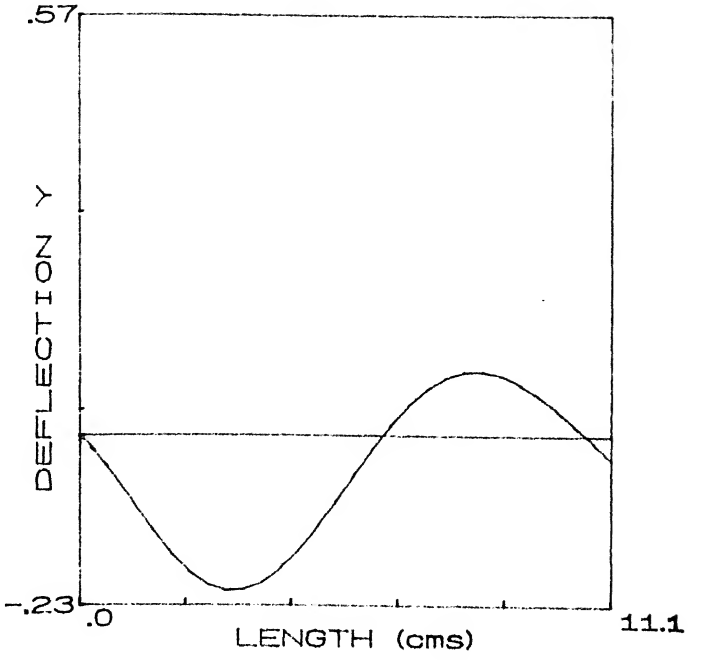

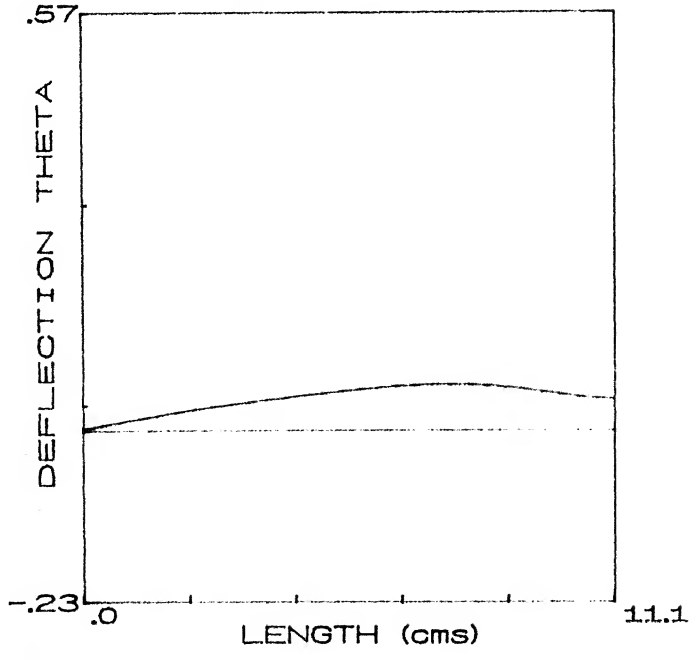

MODE # 5

NATURAL FREQUENCY (Hz): .97438E+04

Fig. 3.7e Mode shapes

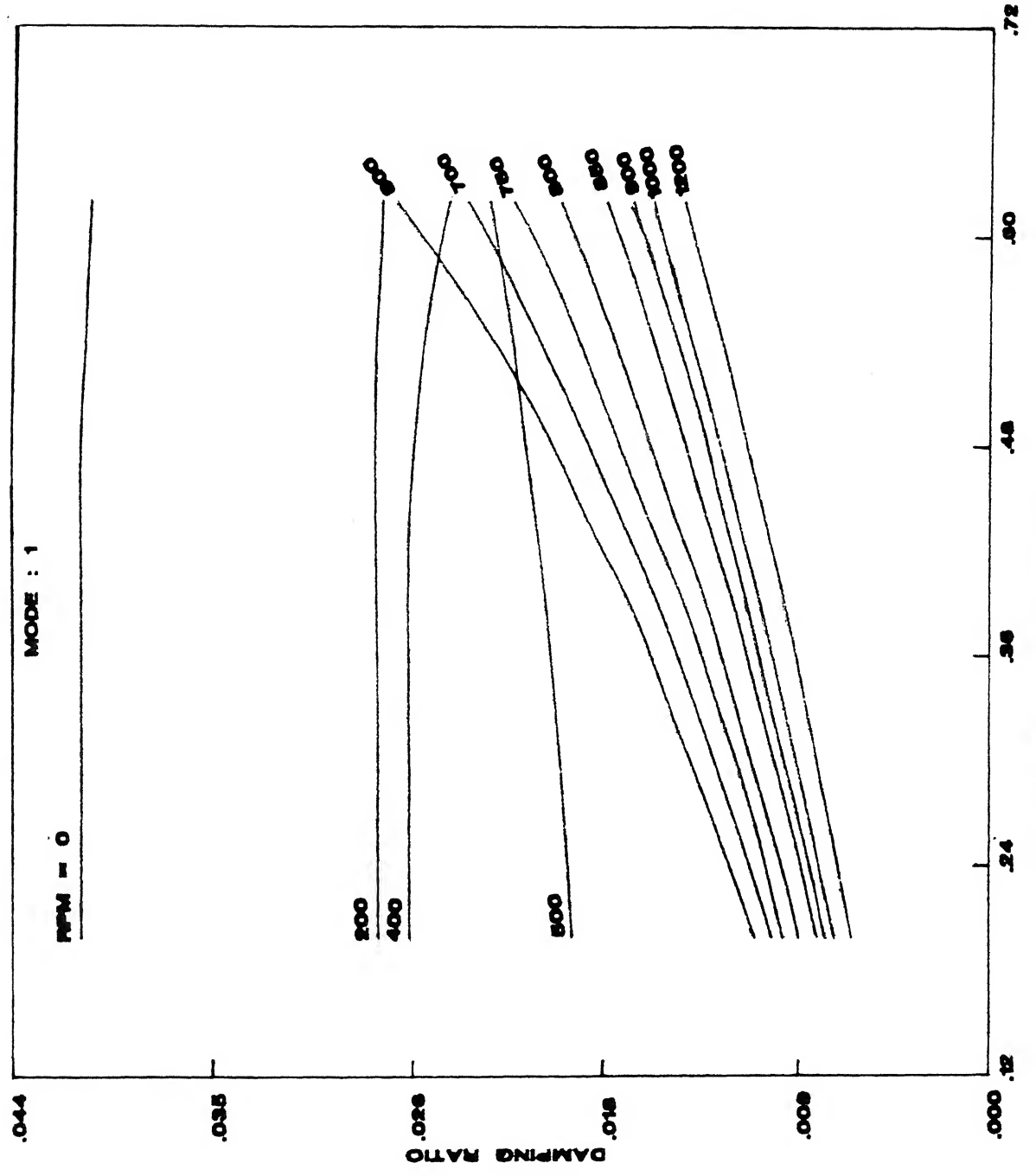

Fig. 3.8 Damping ratio vs strain amplitude - Mode I

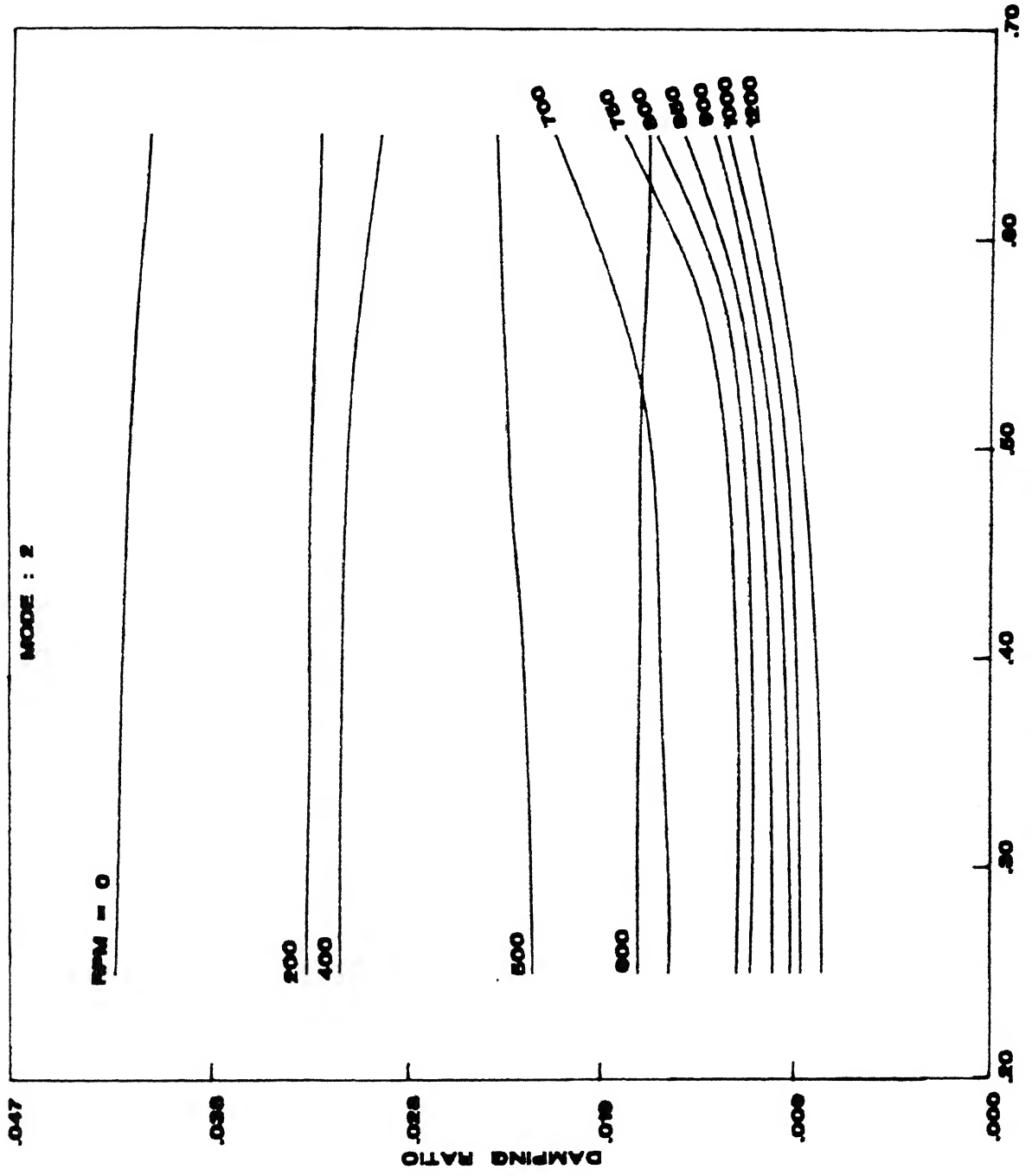

Fig. 3.9 Damping ratio vs strain amplitude - Mode II

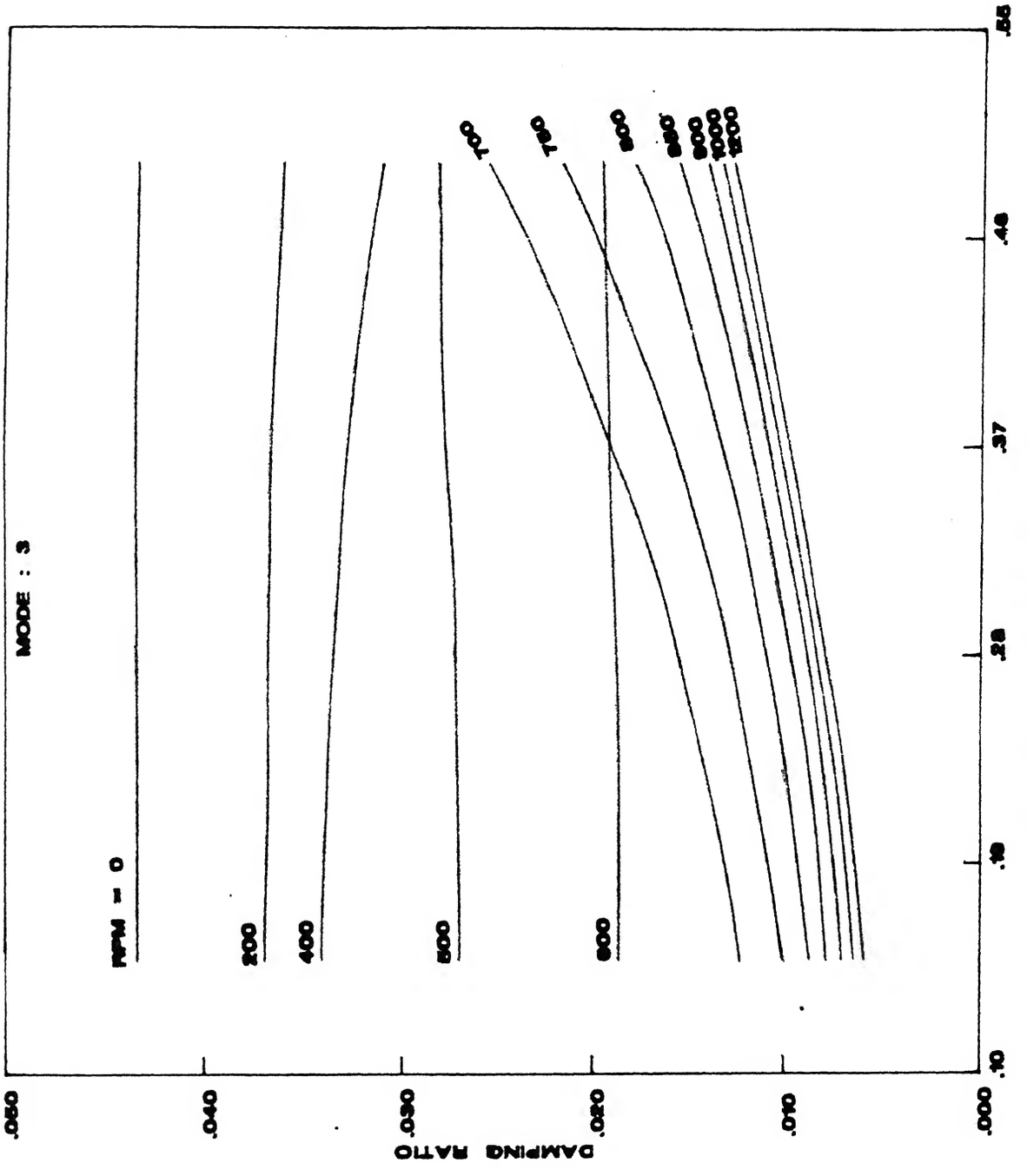

Fig. 3.10 Damping ratio vs strain amplitude - Mode III

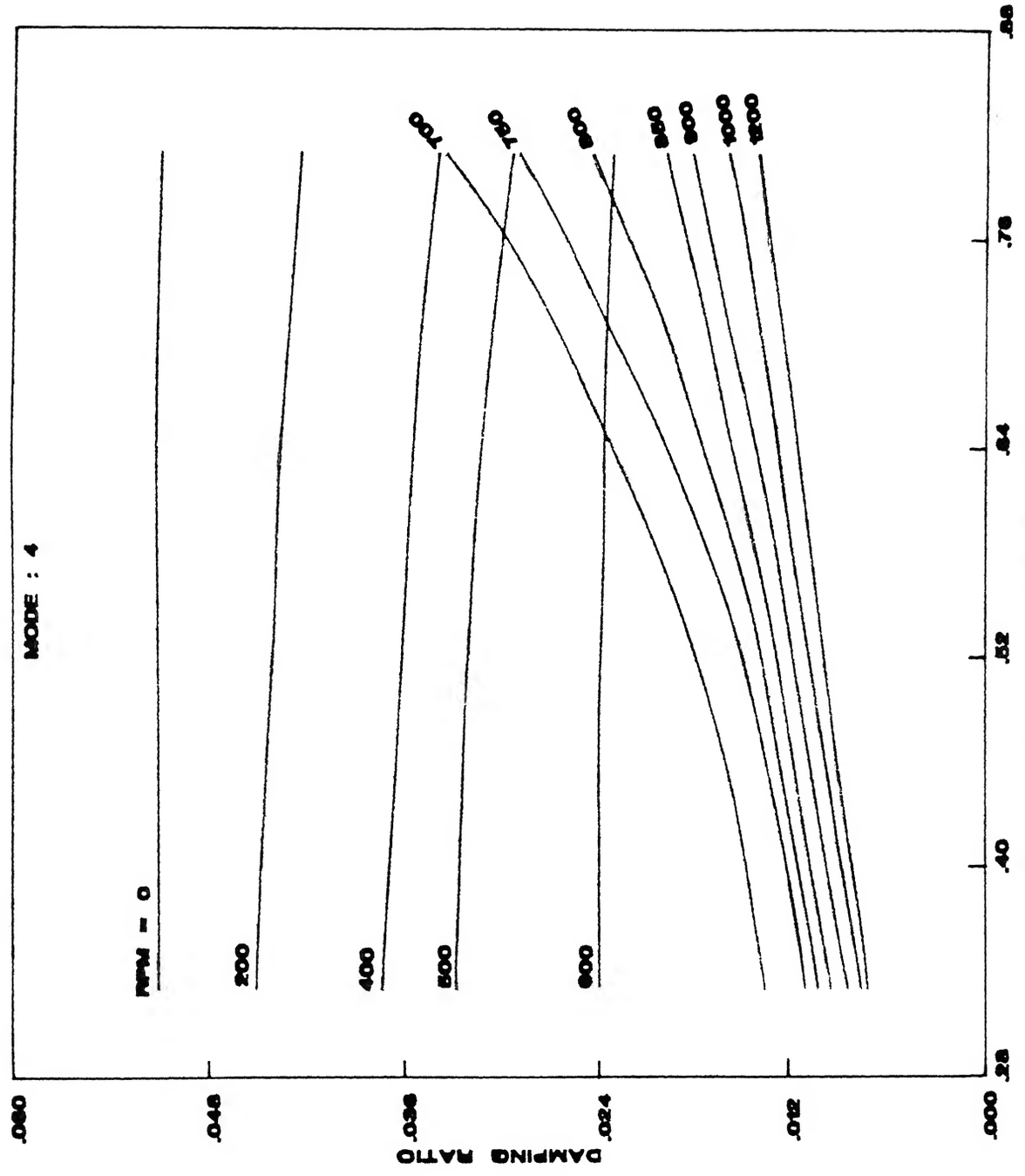

Fig. 3.11 Damping ratio vs strain amplitude - Mode IV

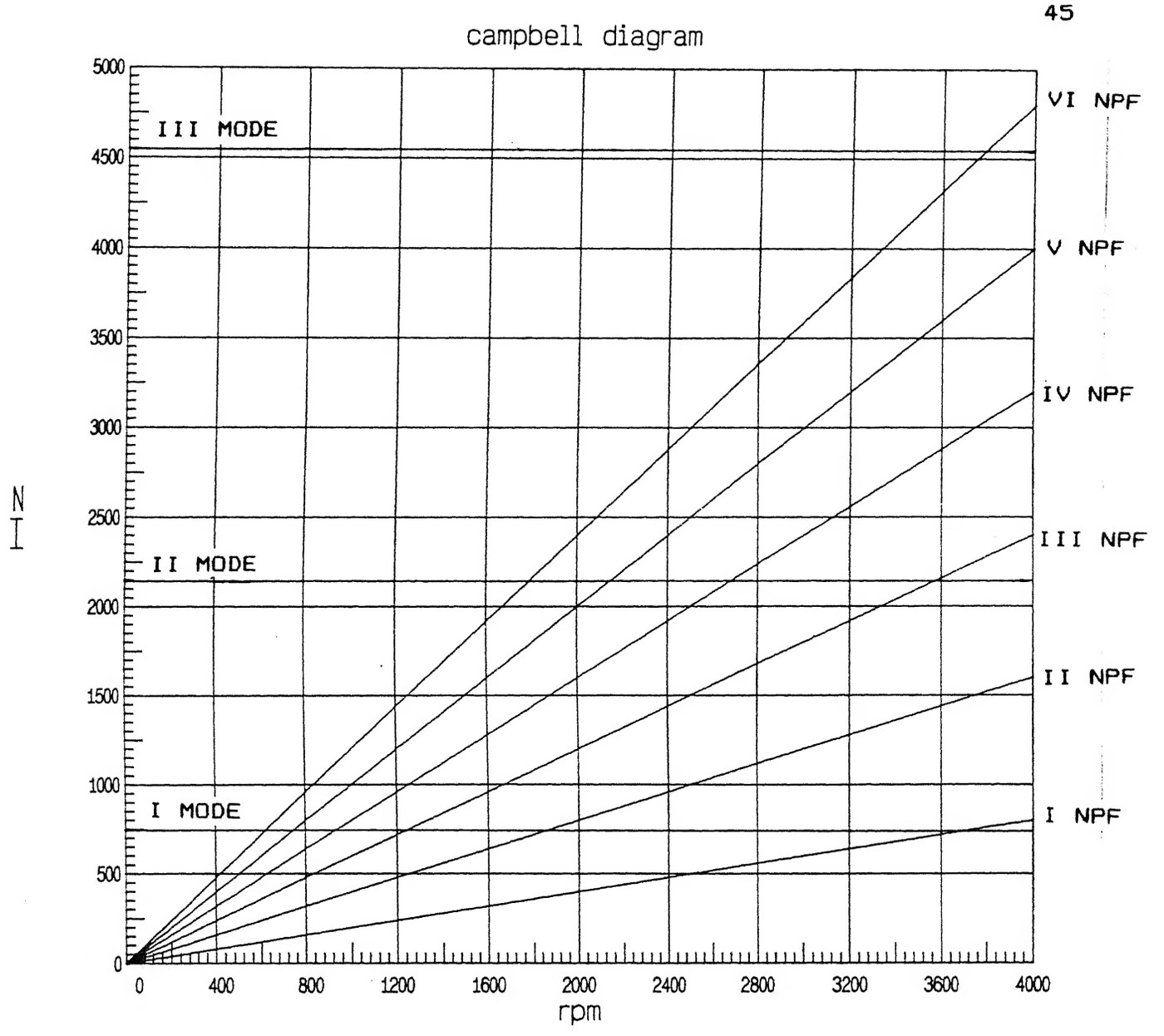

Fig. 3.12 Campbell diagram

TABLE 3.2

RESONANT ROTOR SPEEDS (RPM)

NPF ORDER	FIRST COUPLED MODE	SECOND COUPLED MODE	THIRD COUPLED MODE
I	3718.2	—	—
II	1859.1	—	—
III	1239.4	3572.8	—
IV	929.5	2683.6	—
V	743.2	2146.5	—
VI	619.3	1788.8	3790.8

"—" INDICATES THAT THE VALUE LIES BEYOND 4000 RPM

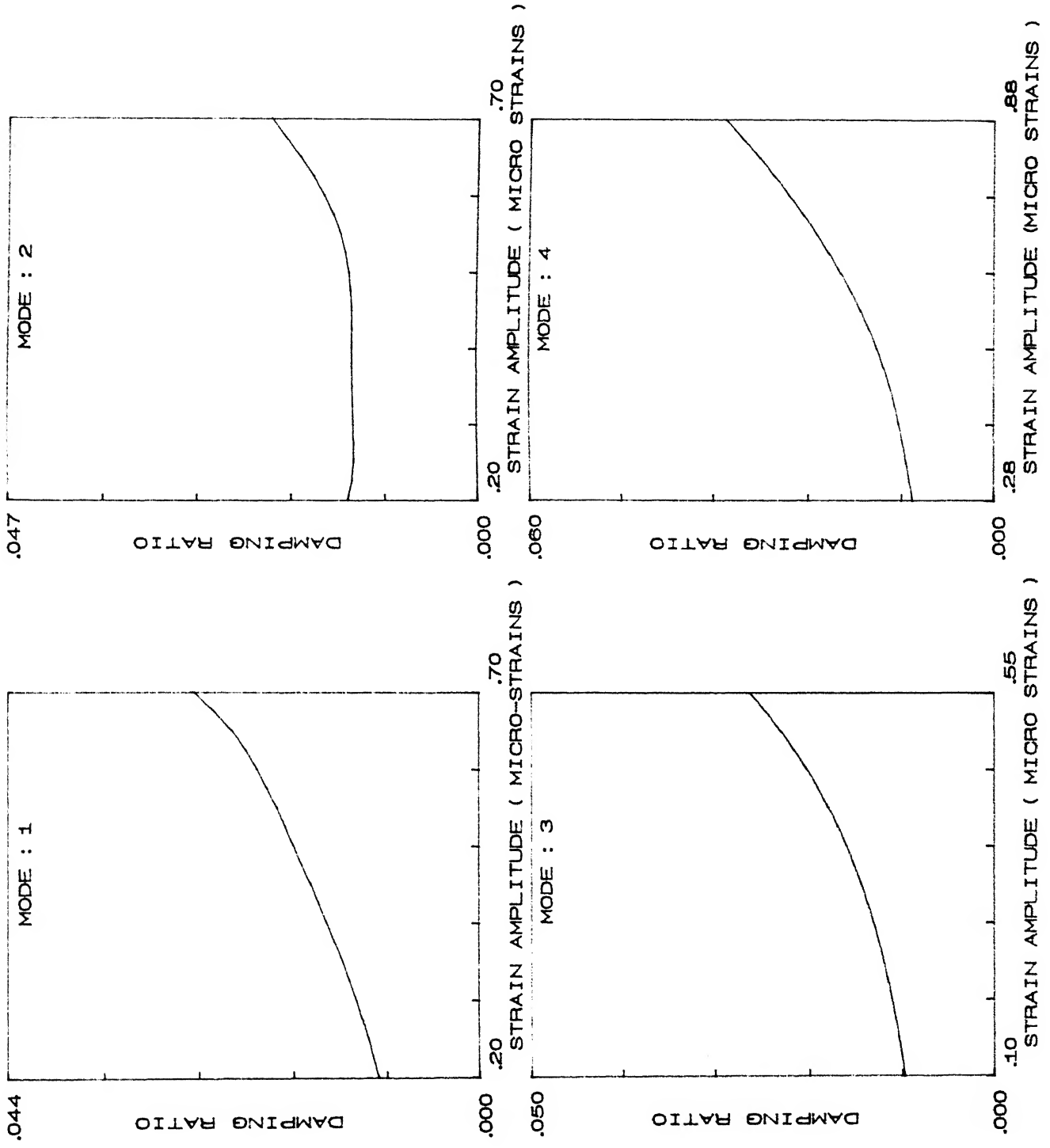

Fig. 3.13 Damping curve for 619 rpm

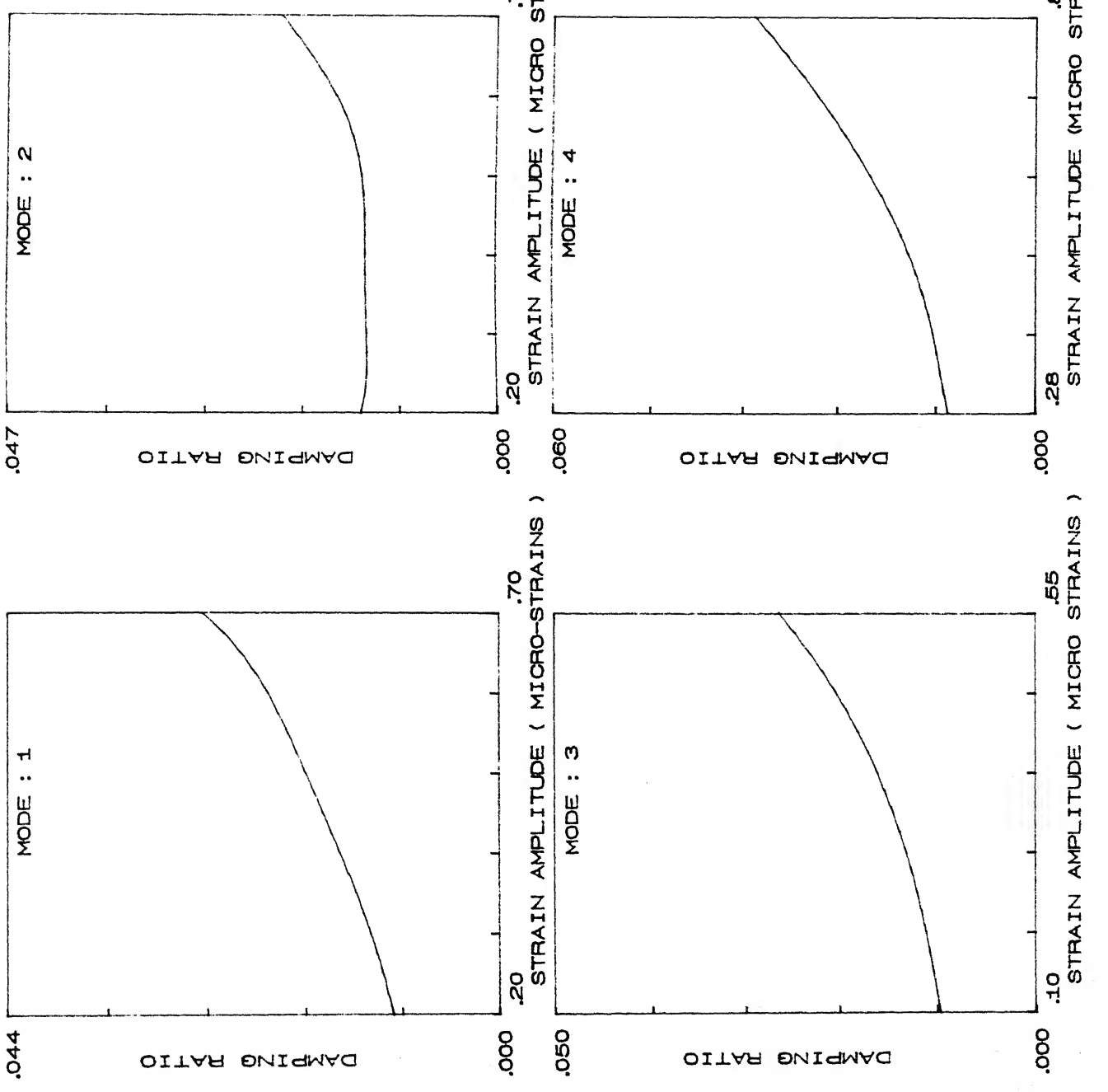

Fig. 3.14 Damping curve for 743 rpm

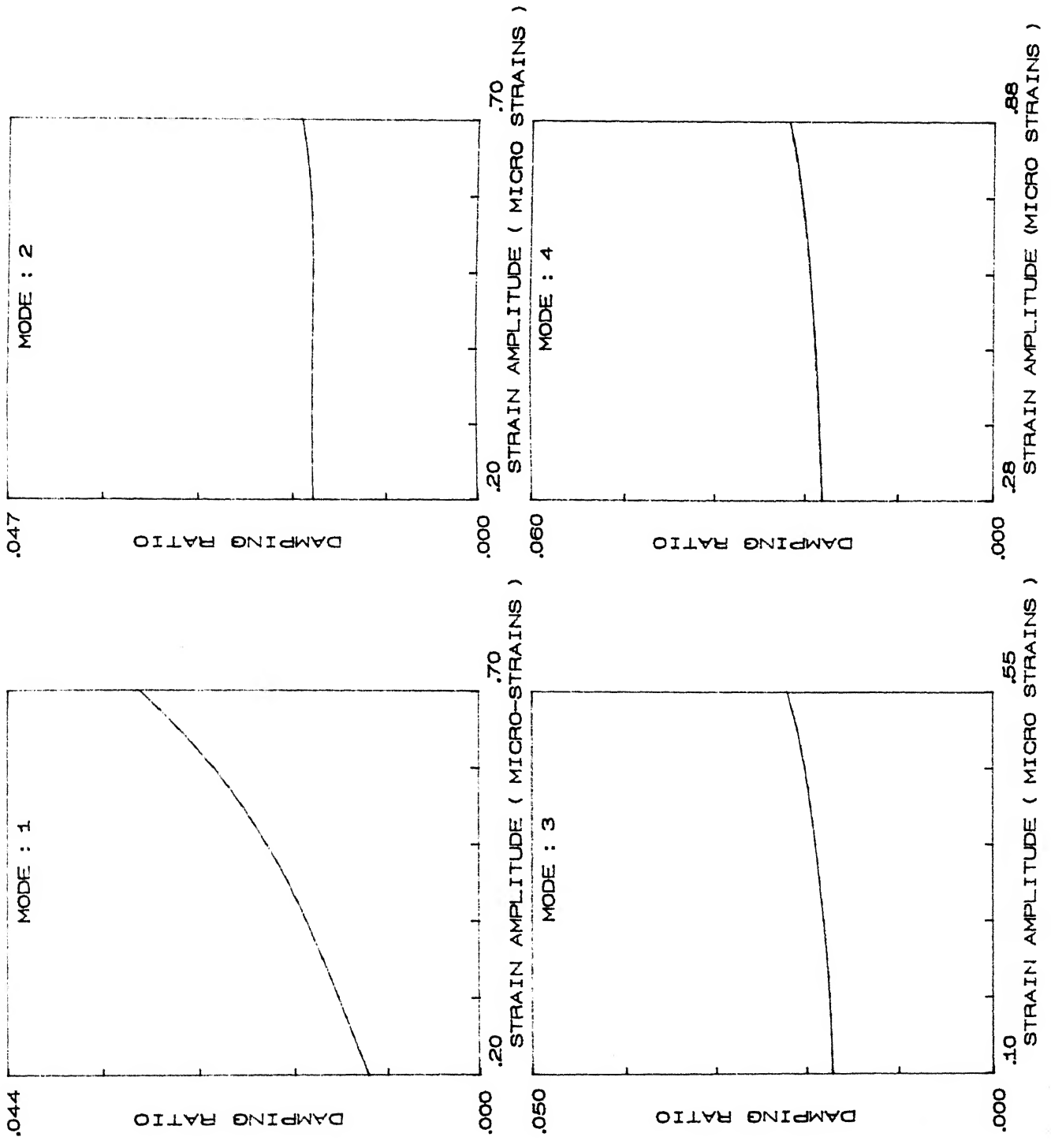

Fig. 3.15 Damping curve for 930 rpm

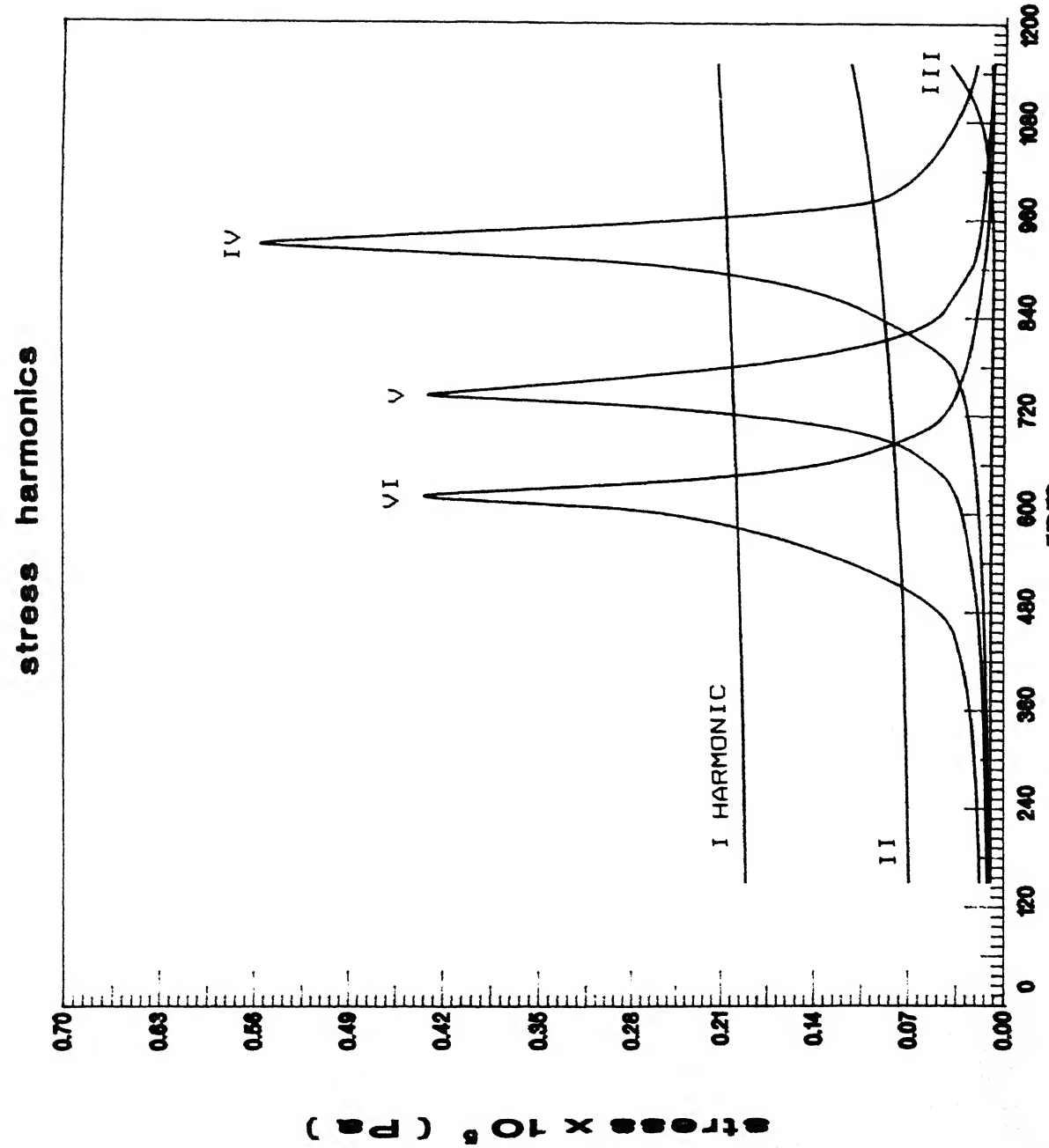

Fig. 3.16 Stress harmonics

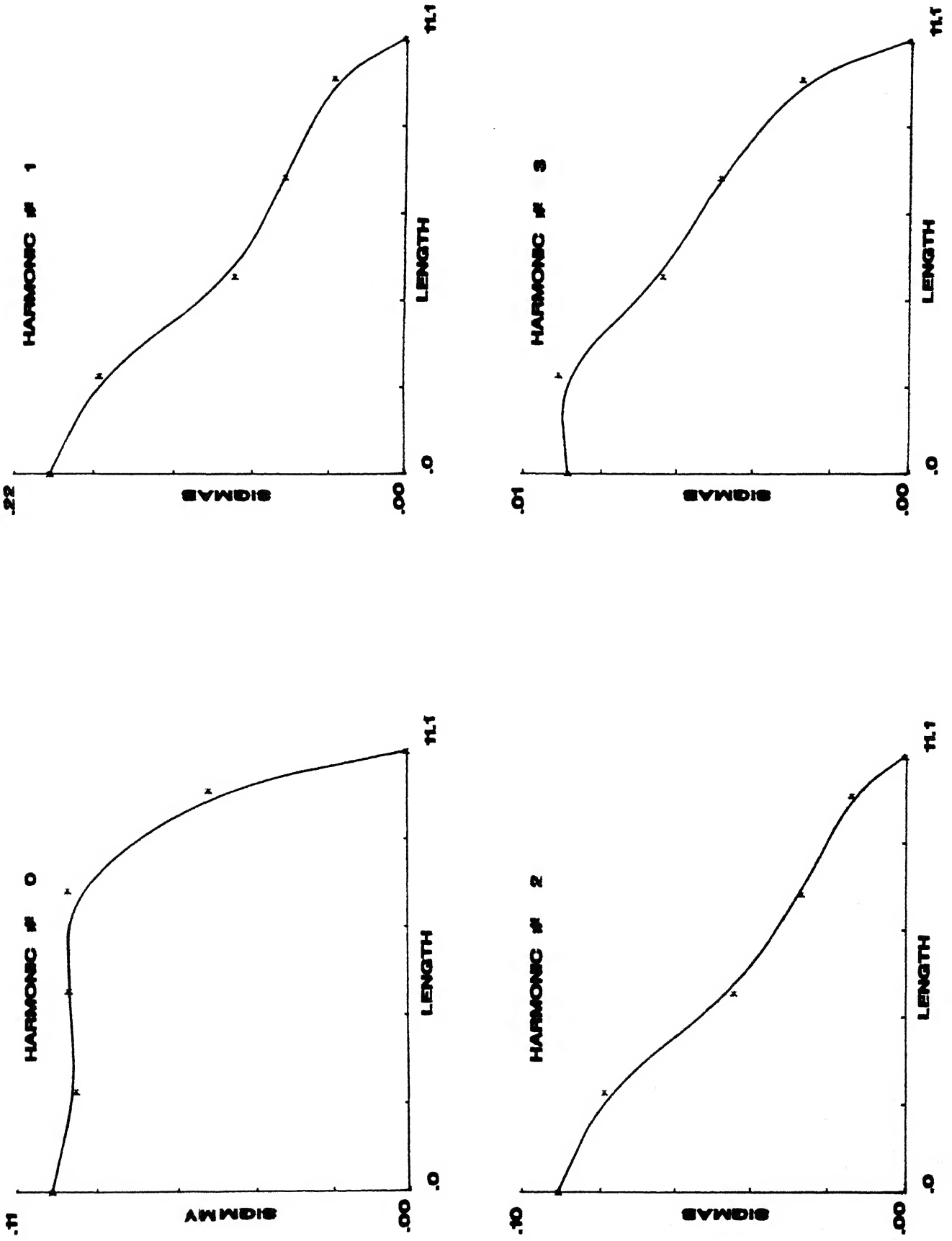

Fig. 3.17a Stress harmonics vs blade length at 930 rpm

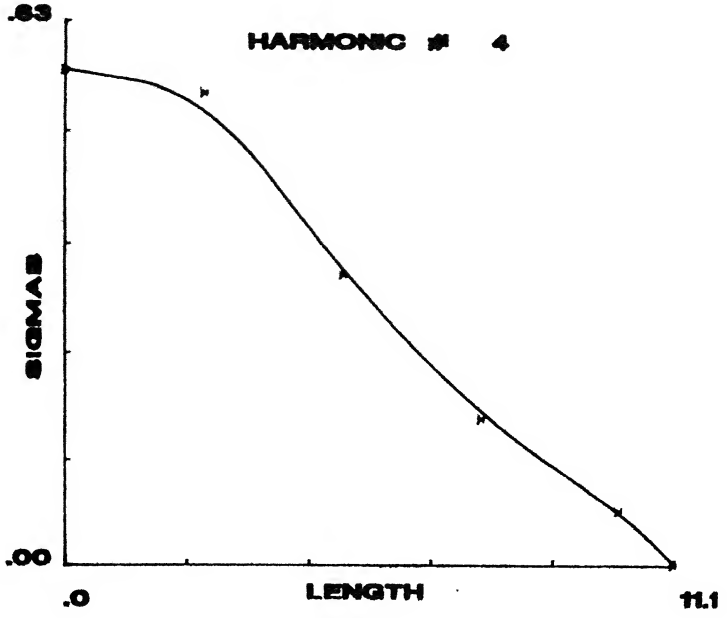

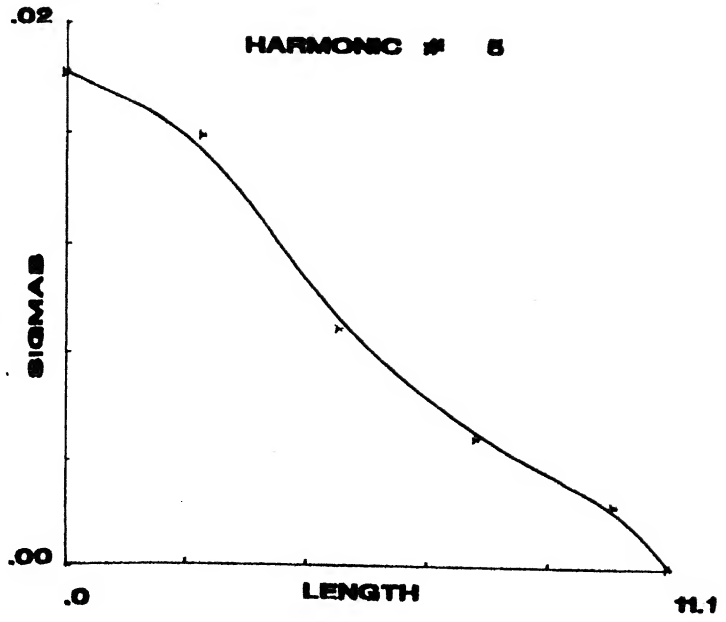

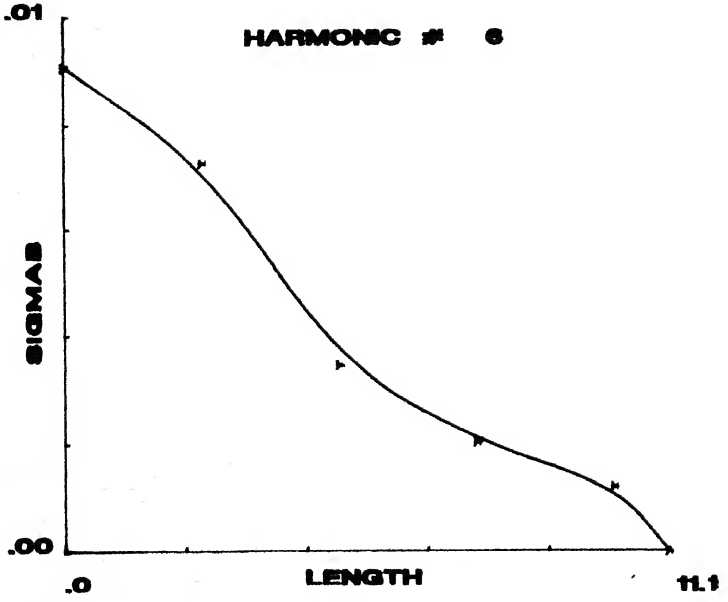

CENTRAL LIBRARY
I.I.T., KANPUR
Acc. No. A.113372

Legend

SIGMAB Basic Vibratory Stress due to non zeroth harmonic component of force

SIGMAMV mean stress due to zeroth harmonic component of force

Fig. 3.17b Stress harmonics vs blade length at 930 rpm

CHAPTER 4

LIFE ESTIMATION

Blade fatigue is strongly influenced by the mean and alternating stresses experienced during operation, by the elastic and fatigue properties of the blade material and chemistry of the operating environment. The critical aspect of the problem constitutes occurrence of large dynamic stresses due to resonant or near resonant vibration at some engine harmonic. Large dynamic stresses, thus, get inflicted on the blade. The damaging fatigue influences cumulate to "initiate" a crack in a zone of high stress, at some metallurgical or structural discontinuity, and if critical conditions of blade operations sustain, the crack "propagates" to lead to failure. Reference can be made to article by Dewey and Rieger [22] for a survey of the nature and extent of some recent specific industrial turbine blade failures.

It becomes imperative to correlate blade vibrations to blade fatigue in order to assess the residual life of the existing blading and for the development of newer blade designs.

Prediction of blade residual life requires :

(a) Stress loading history of the blade.

(b) Material strength and life properties.

(c) Life estimation algorithm.

These aspects have been discussed by Rao and Vyas [1] and blade life has been estimated using stress based approach ie. von Mises theory with the S-N mean stress diagram. Recently, Irretier presented a life estimation model based on different stress approaches to cumulative damage and discussed related numerical studies.

These approaches, however, suffer from a drawback that they do not make allowance for the possibility of the development of plastic strain zones, especially in cases of low cycle fatigue. In this context, Rieger [17] and has pointed to the need for development of a fatigue model based on more fundamental and modern "fracture mechanics" concepts.

In the present study, an attempt has been made to develop a life prediction algorithm based on fracture mechanics and strain-life approach. In order to duly analyse "crack initiation" and "crack propagation", a combination approach, originally proposed by Dowling [23] for notched members and modified by Socie [24], has been employed.

The method consists of the following :

Crack Initiation

(1) Starting from a nominal stress (from stress analysis), determination of elasto-plastic strain using Nueber's rule [25].

(2) Coupling with material hysteresis curve and Massing's hypothesis [26] and solving for plastic stress through

iterative technique.

(3) Accounting for mean stress by Morrow's hypothesis [27] and determination of crack initiation life.

Crack propagation

(1) Determination of propagation life using Paris equation [28].

(2) Employing the method of Socie et al [24] in neglecting an estimate of the characteristic crack length.

The method is outlined in more detail in Fig. 4.1.

However, for the purpose of numerical demonstration of the method, a number of approximations have been made regarding the fatigue data. This has been essential due to lack of better criterion. The approximations have been stated explicitly whenever made. It is also to be realised that fatigue failure being a statistical process, experimental validation of life algorithms in real life situations proves to be prohibitively expensive. With the present state of art, real life turbine blading failure problems are being dealt only through approximate thumb rule predictions.

In this context, the present model is to be viewed, not as an exact closed form solution of the problem but as an improvement on the existing conventional stress based approach.

The various aspects of the methodology are described in the following sections.

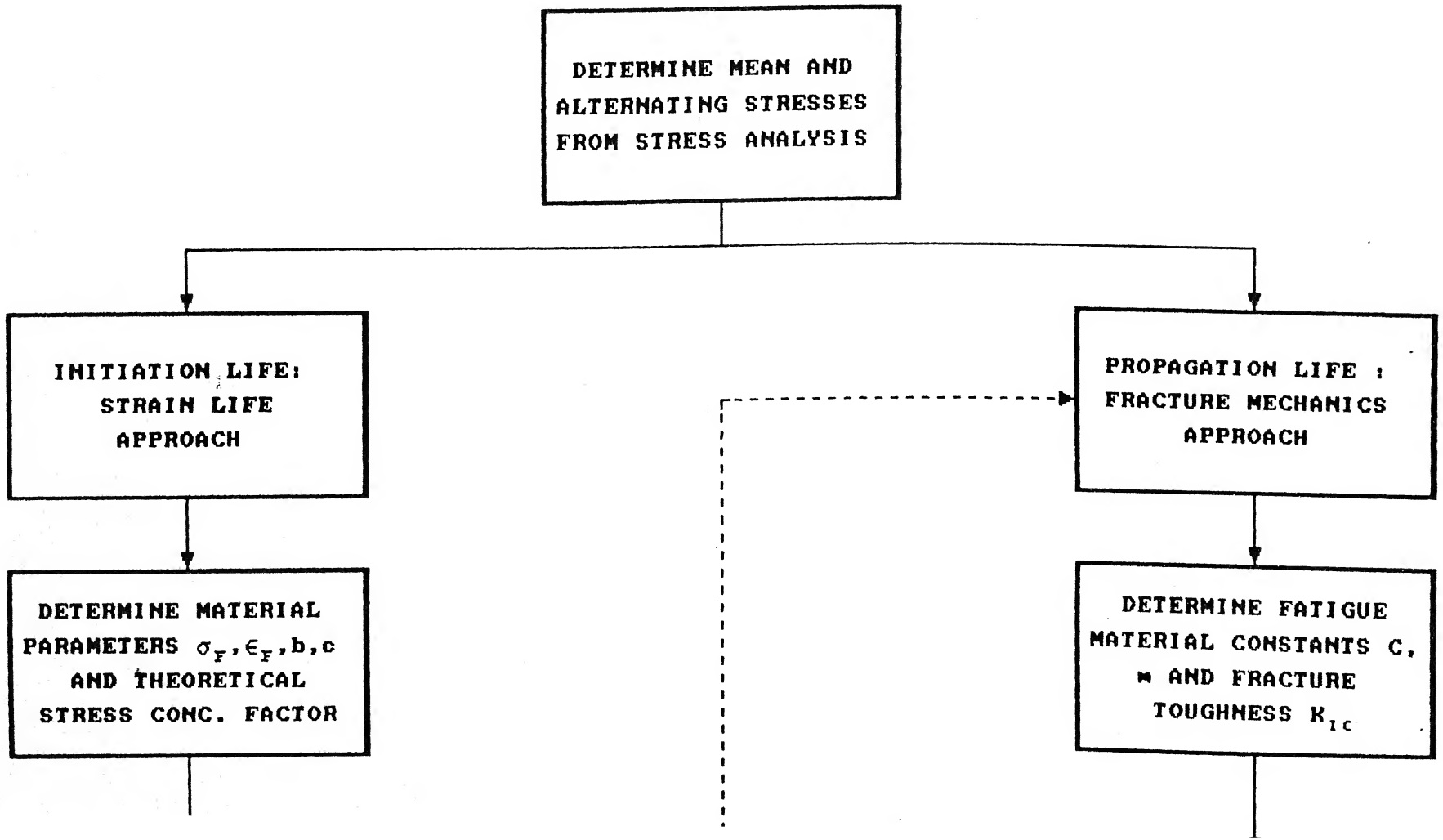
DETERMINE MEAN AND ALTERNATING STRESSES FROM STRESS ANALYSIS
INITIATION LIFE: STRAIN LIFE APPROACH
PROPAGATION LIFE : FRACTURE MECHANICS APPROACH
DETERMINE MATERIAL PARAMETERS σ_F, ϵ_F, b, c AND THEORETICAL STRESS CONC. FACTOR
DETERMINE FATIGUE MATERIAL CONSTANTS C, m AND FRACTURE TOUGHNESS K_{IC}

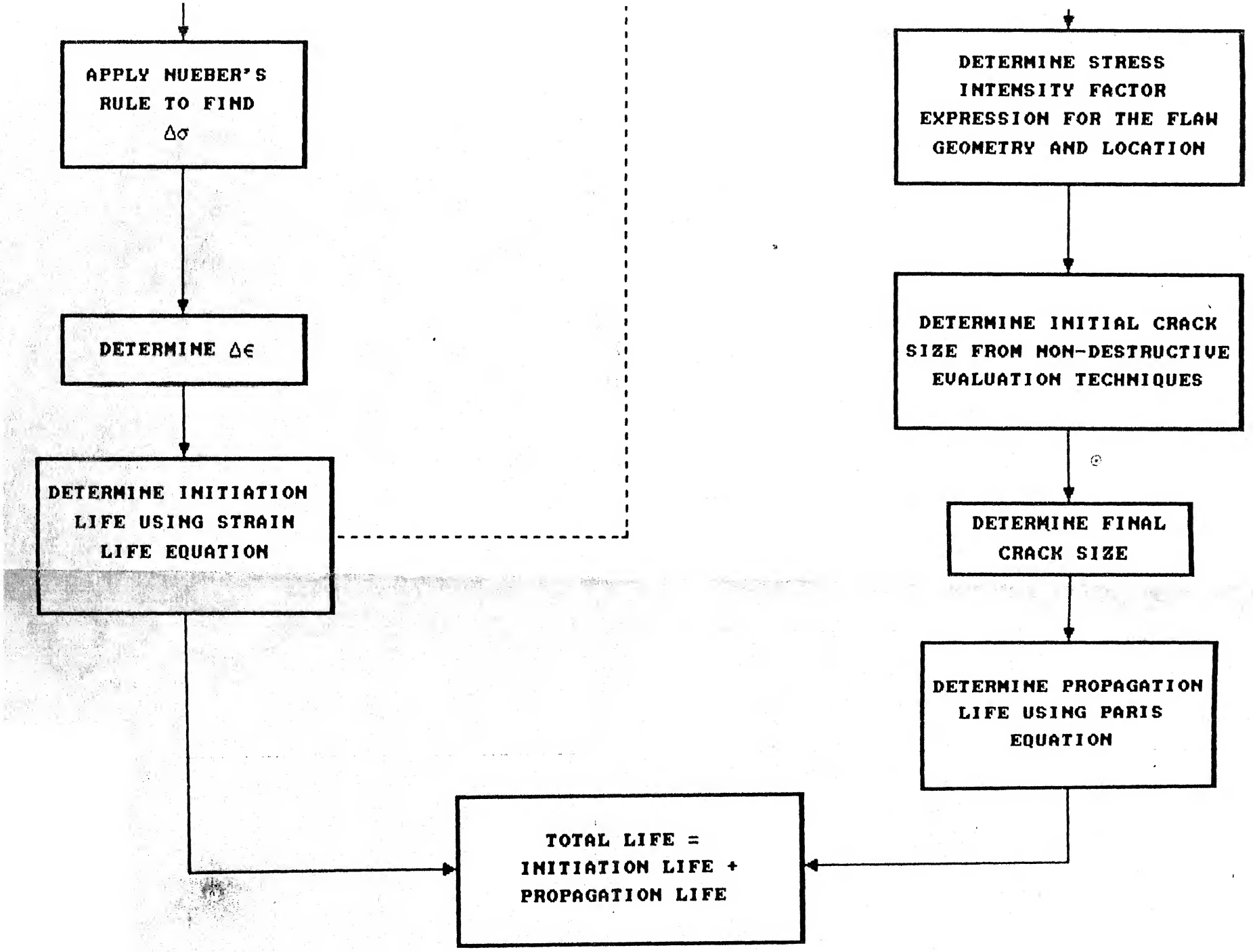

FIG. 4.1 LIFE PREDICTION ALGORITHM

4.1 STRAIN-LIFE APPROACH FOR CRACK INITIATION

This approach is based on the observation that in many components, the response of the material in critical locations (notches and flaws) is strain dependant. This is specially true for low cycle fatigue regime. In the strain life approach the plastic strain is quantified and therefore removes the drawback of the S-N approach which considers stresses and strains to be elastic. At long lives, where plastic strain is negligible, the stress life and strain- life approaches are essentially the same.

Although most engineering components are designed such that nominal loads remain elastic, stress concentrations often cause plastic strains to develop in the vicinity of notches and cracks. Due to the constraint imposed by the elastically stressed material surrounding the plastic zone, the deformation at the notch is considered strain controlled. The strain-life method assumes that the smooth specimens tested under strain controlled conditions can simulate fatigue damage at the notch root of an engineering component. Crack growth is, however, not explicitly accounted for in this method and the need arises to go in for the fracture mechanics approach for crack propagation life estimates.

4.1.1 Stress - strain relationships

Total strain = Elastic strain + Plastic strain

$$\epsilon_t = \epsilon_e + \epsilon_p \qquad (4.1)$$

For most metals, a log-log plot of the true stress versus true

plastic strain is modelled as a straight line. Therefore,

$$\epsilon_p = \left[\frac{\sigma}{K} \right]^{1/n} \tag{4.2}$$

and the expression for total strain is

$$\epsilon_t = \frac{\sigma}{E} + \left[\frac{\sigma}{K} \right]^{1/n} \tag{4.3}$$

4.1.2 Cyclic stress - strain behaviour

The response of a material subjected to cyclic inelastic loading is in the form of a hysteresis loop as shown in Fig. 4.2. The relation between the total strain range, elastic strain range and the plastic strain range is

$$\Delta\epsilon = \Delta\epsilon_e + \Delta\epsilon_p \tag{4.4}$$

or,

$$\frac{\Delta\epsilon}{2} = \frac{\Delta\sigma}{2E} + \frac{\Delta\epsilon_p}{2} \tag{4.5}$$

A comparison between the monotonic and cyclic stress-strain curve provides a quantitative assessment of the cyclically induced changes in the mechanical behaviour. The potential danger of using monotonic properties to predict cyclic strains is pointed out in [29]. The monotonic properties may predict strains that are fully elastic, when in fact the material may experience large amounts of cyclic plastic strains. Therefore, whenever available, the cyclic stress-strain data should be used for cyclic loading.

4.1.3 Stress - plastic strain law

Analogous to the monotonic stress-strain curve, a log-log plot of the completely reversed stabilised cyclic true stress versus true plastic strain can be approximated by a straight line and a similar power law function is used,

$$\sigma = K' (\epsilon_p)^{n'} \tag{4.6}$$

$$\epsilon = \frac{\sigma}{E} + \left[\frac{\sigma}{K'} \right]^{1/n'} \tag{4.7}$$

The equation of the hysteresis loop can be derived from the equation of the cyclic stress-strain curve using Massing's hypothesis [26]. This allows the stabilised hysteresis loop to be determined for a material that exhibits symmetric behaviour in tension and compression. This hypothesis states that the stabilised hysteresis loop may be obtained by doubling the cyclic stress-strain value from the stabilised cyclic stress-strain curve. The equation of the hysteresis loop can, now be written as

$$\frac{\Delta\epsilon}{2} = \frac{\Delta\sigma}{2E} + \left[\frac{\Delta\sigma}{2K'} \right]^{1/n'} \tag{4.8}$$

4.1.4 Geometry effects

The fatigue resistance of most metals is affected by the geometric conditions. Stress concentration is evidenced due to surface discontinuities such as notches, holes and scratches. The stress concentration factor, K_t, is dependant on the geometry and the mode of loading and its values are compiled in various texts, the most popular and well used being that of Peterson's [30].

Tests of notched specimens usually result in fatigue lives which are greater than those using K_t and for this reason a fatigue notch factor, K_f, has been defined. In accordance with the approximations suggested by Socie [24], which will be discussed in a later section, the theoretical stress concentration factor, K_t, will be used for formulation and computation.

4.1.5 Nueber's rule

Nueber [25] analysed a specific notch geometry and obtained his rule. Although his method was proved only for one notch geometry, it is assumed that his relationship holds true for most notch geometries[29]. The rule states that the theoretical stress concentration is the geometric mean of the strain and stress concentration, ie.

$$K_t = (K_\sigma K_\epsilon)^{1/2} \qquad (4.9)$$

where,

K_σ : stress concentration factor $= \frac{\sigma}{S}$

K_ϵ : strain concentration factor $= \frac{\epsilon}{e}$

or,

$$K_t^2 = K_\sigma K_\epsilon \qquad (4.10)$$

When nominal strains are elastic, the nominal stress, S, and nominal strain, e, are related by Hooke's law. The Nueber's rule then becomes

$$\frac{(K_t S)^2}{E} = \sigma \epsilon \qquad (4.11)$$

If nominal strains are inelastic different version of Nueber's rule must be used. For the purpose of this analysis it is assumed that nominal strains are elastic.

In terms of the stress and strain amplitudes, Nueber's rule can be written as

$$\Delta\sigma \, \Delta\epsilon = \frac{(K_t \Delta S)^2}{E} \qquad (4.12)$$

Substituting the value of $\Delta\epsilon$ from equation (4.8) the Nueber's rule becomes

$$\Delta\sigma \left\{ \frac{\Delta\sigma}{E} + 2 \left[\frac{\Delta\sigma}{2K'} \right]^{1/n'} \right\} = \frac{(K_t \Delta S)^2}{E} \qquad (4.13)$$

4.1.6 Strain life equation

Basquin [31] observed that stress life (S-N) data could be plotted linearly on a log-log scale. Hence,

$$\frac{\Delta\sigma}{2} = \sigma_f' (2N_f)^b \qquad (4.14)$$

where,

$\frac{\Delta\sigma}{2}$: true stress amplitude

$2N_f$: reversals to failure

σ_f' : fatigue strength coefficient

b : fatigue strength exponent

σ_f' and b are fatigue properties of the material, whose definition and determination is the subject of discussion of the immediate section.

Also, Coffin [32] and Manson [33], working independently, found that plastic strain-life data could be linearised on log-log scale. Therefore,

$$\frac{\Delta\epsilon_p}{2} = \sigma_f' \, (2N_f)^b \qquad (4.15)$$

where,

$\frac{\Delta\epsilon_p}{2}$: plastic strain amplitude

ϵ_f' : fatigue ductility coefficient

c : fatigue ductility exponent

The total strain amplitude can now be written as

$$\frac{\Delta\epsilon}{2} = \frac{\sigma_f'}{E} (2N_f)^b + \epsilon_f' (2N_f)^c \qquad (4.16)$$

The above equation (4.16) is known as Strain-life equation.

4.1.7 Determination of fatigue parameters

The strain based approach to fatigue requires five parameters, namely σ_f', ϵ_f', b, c and E.

Fatigue strength coefficient, σ_f', is the intercept of the true stress amplitude - fatigue life (reversals to failure) plot at one reversal. This is determined by curve fit of actual experimental data. In the absence of actual tests a fairly good approximation is $\sigma_f' \cong \sigma_f$ (true stress at fracture). For steels with hardness below 500 HB it may be approximated as

$$\sigma_f' \cong S_u + 345 \quad (\text{in MPa})$$

where S_u is the ultimate tensile strength.

Fatigue strength exponent, b, is the exponent obtained on curve fitting experimental cyclic fatigue data. Its value varies from -0.05 to -0.12 for most metals with an average value of -0.085.

Fatigue ductility coefficient, ϵ_f', is approximated by the true fracture ductility ie.

$$\epsilon_f' \cong \epsilon_f = \ln \frac{1}{1 - RA}$$

where RA is the percentage reduction in area.

Fatigue ductility exponent, c, is not as well defined as others and a rule of thumb has to be followed for its estimation. Its value has been found by Coffin to be about -0.5, by Manson to be about -0.6 and by Morrow to be lying between -0.5 and -0.7. The values of these parameters have been compiled such as those in [34].

4.1.8 Mean stress effects

Cyclic fatigue properties of a material are obtained from completely reversed, constant amplitude strain controlled tests. Mean stress is usually present in most practical situations. Mean stress can either increase the fatigue life, when compressive, or decrease it when tensile.

The strain life equation is therefore modified, to include mean stress effects, as suggested by Morrow [27]

$$\frac{\Delta\epsilon}{2} = \frac{\sigma_f' - \sigma_m}{E} (2N_p)^b + \epsilon_f' (2N_p)^c \qquad (4.17)$$

in which σ_m is the mean stress.

The predictions made with this equation are consistent with the

observation that mean stress effects are significant at low values of plastic strain, where elastic strains dominate. They also reflect the trend that mean stresses have little effect at shorter lives, where plastic strains are large. However, it incorrectly predicts that the ratio of elastic to plastic strain is dependant on the mean stress. Despite this drawback, it gives a fairly good life estimate.

4.2 FRACTURE MECHANICS APPROACH FOR CRACK PROPAGATION

Linear elastic fracture mechanics (LEFM) is based on the application of the theory of elasticity to bodies containing cracks or defects. As materials plastically deform, when the yield stress is exceeded, a plastic zone is formed near the crack tip. The basis of LEFM remains valid if this region of plasticity remains small in relation to the overall dimensions of the crack and the crack body.

4.2.1 Stress Intensity Factor and Fracture Toughness

Stress intensity factor defines the magnitude of the local stresses around a crack tip. THis factor depends on the loading, crack size, crack shape and geometric boundaries. Its general form is given by

$$K = F \sigma \sqrt{\Pi a} \qquad (4.18)$$

where,

σ : remote stress applied to the component

a : instantaneous crack length

F : correction factor that depends on the specimen and crack geometry

Stress Intensity Factor solutions have been obtained for a wide variety of problems and published in handbooks eg. [35]. Finite element and other numerical methods are widely used for determination of K.

As the stress intensity factor reaches a critical value, K_c, unstable fracture occurs. This critical value of stress intensity factor, known as fracture toughness of the material, is a mechanical property measuring resistance to cracking under load. The plain strain fracture toughness, K_{IC}, is dependant on specimen geometry and metallurgical factors. ASTM E399, Standard Method of Test for Plain Strain Fracture Toughness of Metallic Materials, sets forth accepted procedures for determining this value.

4.2.2 Fatigue crack growth

The Paris equation [28] is used to predict the number of cycles spent in the growth of the crack to some specified length. In this equation

$$\frac{da}{dN} = C (\Delta K)^m \qquad (4.19)$$

in which C and m are material constants and ΔK the stress intensity factor range. These material constants, C and m, are determined by curve fit of experimental data and are available for some steels in literature eg.[34]. ASTM E647 sets guidelines for determining these.

Using Paris formulation, the crack growth life, in terms of cycles to failure, may be written as

$$N_p = \int_{a_i}^{a_f} \frac{da}{C\ (\ \Delta K\ )^m} \qquad (4.20)$$

in which a_i and a_f are the initial and final crack lengths respectively. The equation (4.20) can be solved numerically. Before it can be solved the final crack size, a_f, must be estimated using

$$a_f = \frac{1}{\Pi} \left[\frac{K_c}{\sigma F} \right]^2 \qquad (4.21)$$

F varies with crack length, a, and iterative procedure are required to solve for the final crack size.

4.3 COMBINATION METHOD

Dowling [23] proposed a method, which combines local strain approach to predict initiation life and fracture mechanics approach to predict propagation life, to estimate the total fatigue life of a notched component. He proposed that within a distance from the notch, l_t, the local notch stress field dominates the stress intensity solution. When the crack is smaller than this length ($l < l_t$) crack initiation can be estimated using the strain-life approach. Use of this approach to estimate the initiation life avoids the inherent difficulty of LEFM to describe short crack behaviour at the notch root. The basic assumption of LEFM, that the plastic zone size is small compared to the crack length, is violated for short cracks. Once the crack is larger than this length ($l > l_t$) crack growth can be modelled with the fracture mechanics approach. Therefore total life is given by

$$\text{Total life} = \underset{(l < l_t)}{\text{Initiation life } (N_i)} + \underset{(l > l_t)}{\text{Propagation life } (N_p)}$$

STRAIN LIFE APPROACH FRACTURE MECHANICS APPROACH

(4.22)

where the value of a_i for estimation of N_p is given by

$$a_i = D_n + l_t$$

in which D_n is the depth of the notch .

Dowling [23] has given estimates for l_t.

A simpler combined approach that has been shown to yield very similar results to Dowling's method has been proposed by Socie [24]. The implementation in the present work is based on Socie's approach. His method combines

- An initiation life estimate using the strain-life approach that assumes that the notch is fully effective ie. $K_f = K_t$.
- A propagation life estimate obtained, using fracture mechanics approach, that assumes initial crack size equal to the depth of the notch.

This method has simpler implementation since l_t is not to be determined.

4.4 IMPLEMENTATION OF THE ALGORITHM

The algorithm for fatigue life estimation is depicted in the form of a flow chart in Fig.4.1. For the purpose of modelling, a small area in the vicinity of the root is considered as a plate. The width of the plate is taken as the maximum span of the aerofoil cross-section at the base. The plate is assumed to have the same section modulus as the aerofoil section and from this its thickness

is computed. It is assumed that the blade is defect free except for the surface discontinuity of specific nature as analysed in sample case studies. Such discontinuities will invariably occur during the manufacturing of the blade and are modelled as notches. The depth of such a notch is to be determined using non-destructive evaluation techniques for inspection of turbine blades and detection of cracks / flaws. If no crack is detected then the least count of the measurement technique can be taken as the initial depth of the notch. For illustrative case studies, a value of depth of notch equal to 1.0 mm has been taken.

From Fig. 3.16 which depicts the stress harmonics, it is seen that for rotor speeds upto 1200 rpm the root stress is maximum at 930 rpm. It would, therefore, be of interest to estimate the life for the blade rotating at 930 rpm, at which the blade experiences resonant stresses due to the interaction between the first mode and the fourth harmonic of the excitation. The maximum section stresses occur at the root. The total mean stress on the blade comprises of the zeroth harmonic of the stress and the centrifugal stretching of the blade. The centrifugal stresses due to rotation can be determined as

$$\sigma_{mc} = \frac{(R + z)}{A_z} \left(\frac{2\Pi \, RPM}{60} \right)^2 \left(\int_z^1 \rho \, A_z \, dz \right) \qquad (4.23)$$

A computer program based on the algorithm described is developed for estimation of the fatigue life. The blade material chosen is AISI-4340 steel and its properties (from Ref.[14]) used for computation are listed in Table 4.1. The results for the case studies are presented in the next section.

TABLE 4.1

PROPERTIES OF BLADE MATERIAL AISI-4340 STEEL

CYCLIC PROPERTIES	
Modulus of Elasticity (E)	193 GPa
Cyclic Yield Strength (S_{yc})	758 MPa
Cyclic Strain Hardening (n′) Exponent	0.14
Fatigue Strength Exponent (b)	-0.076
Fatigue Ductility Coefficient (ϵ_f')	0.73
Fatigue Ductility Exponent (c)	-0.62
MONOTONIC PROPERTIES	
Ultimate Tensile Strength (S_u)	1241 MPa
Yield Strength (S_y)	1172 MPa
True Fracture stress (σ_f)	1655 MPa
Percentage Reduction (RA)	57 %
True fracture ductility (ϵ_f)	0.84
Strain hardening Exponent (n)	0.066
Strength coefficient (K)	1579 MPa
MATERIAL CONSTANTS	
Fracture Toughness (K_{IC})	137.375 MPa$\sqrt{m}$
C	6.6×10^{-9}
m	2.25

4.5 CASE STUDIES

CASE 1

An initial crack, modelled as a circular notch of radius 1.0 mm, is considered in the blade root section. This is depicted in Fig. 4.3a. For 930 rpm, the stresses obtained from the stress analysis are as follows

Alternating stress (σ_a) = 0.056 MPa

Mean stress due to zeroth harmonic (σ_{mv}) = 0.00986 MPa

Mean stress due to centrifugal effects (σ_{mc}) = 1.044 MPa

Total mean stress = $\sigma_{mv} + \sigma_{mc}$ = 1.05386 MPa

The width of the plate is determined as 3.8 cm and the thickness as 1.0 cm. The theoretical stress concentration factor, K_t, is determined as 3.0. The expression for correction factor F used, is

$$F = \left[\sec \left(\frac{\Pi \, a}{2 \, b} \right) \right]^{1/2}$$

The results of the blade life estimate obtained are as follows

Initiation life estimate = 1.7×10^{52} cycles

Propagation life estimate = 2.2×10^{11} cycles

Total life estimate = 1.7×10^{52} cycles

The total life of the blade is very large since the stresses on the blade are small. This is due to the fact that the nozzle excitation forces due to electromagnetic simulation are very small.

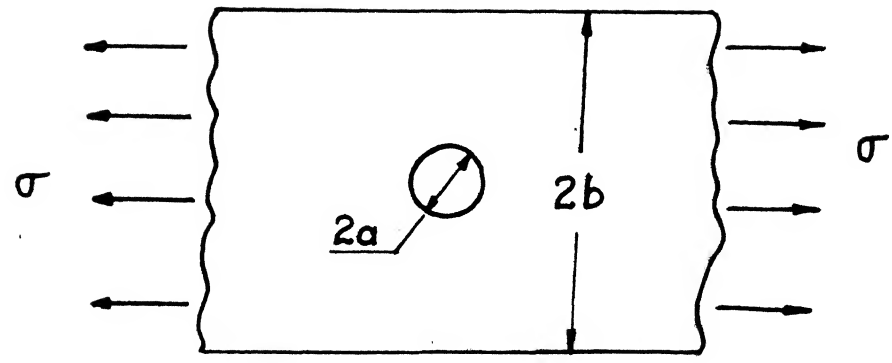

Fig. 4.3a Configuration for Case 1 (not to scale)

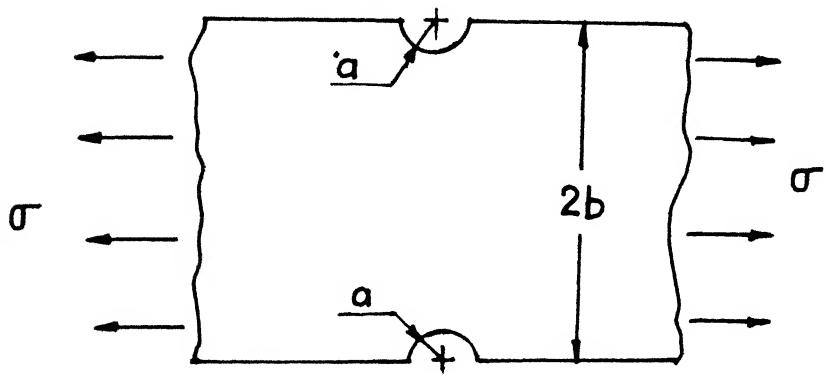

Fig. 4.3b Configuration for Case 2 (not to scale)

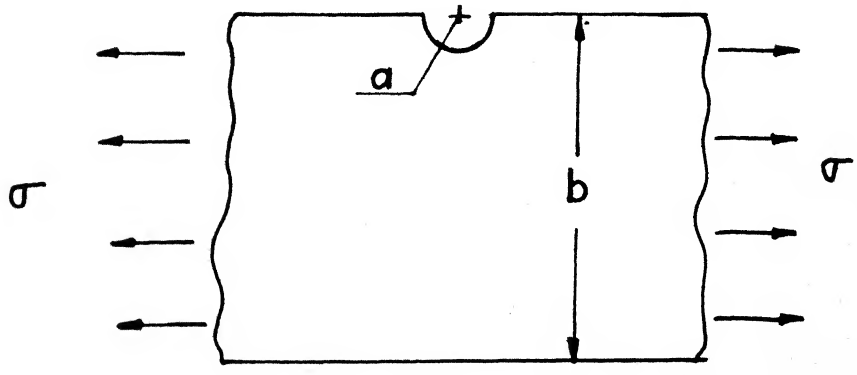

Fig. 4.3c Configuration for Case 3 (not to scale)

In practice, the nozzle forces driving the machine are many times larger and inflict stresses which are considerably greater than those obtained, using available data, in the illustrated case. It is therefore assumed, for furthur illustration, that the forces are such that a thousand times larger stresses are inflicted on the blade. The stresses are now

Alternating stress (σ_a) = 56.0 MPa

Mean stress due to zeroth harmonic (σ_{mv}) = 9.86 MPa

Mean stress due to centrifugal effects (σ_{mc}) = 1.044 MPa

Total mean stress = $\sigma_{mv} + \sigma_{mc}$ = 10.904 MPa

The life estimates obtained are

Initiation life estimate = 0.54×10^{13} cycles

Propagation life estimate = 0.32×10^{5} cycles

Total life estimate = 0.54×10^{13} cycles

CASE 2

Two initial cracks, modelled as two semicircular notches of depth 1.0 mm each, are considered in the blade root section. This is depicted in Fig. 4.3b. For 930 rpm, the stresses obtained from the stress analysis are the same as for Case 1. The theoretical stress concentration factor, K_t, is determined as 3.0. The expression for correction factor used is

$$F = 1.12 + 0.203\left[\frac{a}{b}\right] - 1.197\left[\frac{a}{b}\right]^2 + 1.930\left[\frac{a}{b}\right]^3$$

The results of life estimate obtained are as follows

Initiation life estimate = 0.54×10^{13} cycles

Propagation life estimate = 0.2×10^5 cycles

Total life estimate = 0.54×10^{13} cycles

Comparison between Case 1 and Case 2 reveals that the crack initiation lives in the two cases are the same. This is because the phenomenon of crack initiation is critically dependent on the theoretical stress concentration factor, which is the same in the two cases since the ratio of flaw radius to the blade width is the same in the two cases. The propagation lives, though different, can be seen to be of the same order. On the basis of these observations, it can be stated the size of the flaw is more critical parameter than its location on the blade surface. Such an observation would suit a flaw detection technique whereby in case no flaw is detected, the least count of the detection technique is taken as the flaw size with its location being arbitrary.

CASE 3

An initial crack, modelled as a semicircular notch of depth 1.0 mm, is considered in the blade root section. This is depicted in Fig. 4.3c. the expression for the correction factor used is

$$F = 1.12 - 0.231\left[\frac{a}{b}\right] + 10.55\left[\frac{a}{b}\right]^2 - 21.72\left[\frac{a}{b}\right]^3 + 30.39\left[\frac{a}{b}\right]^4$$

The theoretical stress concentration factor, K_t, is determined to be 2.79. The results of life estimate obtained are as follows

Initiation life estimate = 1.4×10^{13} cycles

Propagation life estimate = 0.17×10^5 cycles

Total life estimate = 1.4×10^{13} cycles

CASE 4

An initial elliptical surface crack into the three dimensional plate is considered (Fig. 4.3d). The correction factor for the stress intensity factor expression has been estimated using empirical relations from [35] . The stress intensity factor for elliptical cracks varies along the periphery and its maximum value has been taken for computation. Two cases, depending on the a/b ratio are considered.

1) Semicircular surface crack with a/b ratio 1.0

The values of a and b are taken as 1.0 mm each for illustration. The correction factor, F, is determined to be 0.732. The life estimates are

Initiation life estimate = 0.76×10^{13} cycles

Propagation life estimate = 0.47×10^{5} cycles

Total life estimate = 0.76×10^{13} cycles

2) Elliptical surface crack with a/b ratio 2.0

The values for a and b are taken as 1.0 mm and 0.5 mm respectively. The value of the correction factor obtained is 0.657. The life estimates are

Initiation life estimate = 0.65×10^{13} cycles

Propagation life estimate = 0.81×10^{5} cycles

Total life estimate = 0.65×10^{12} cycles

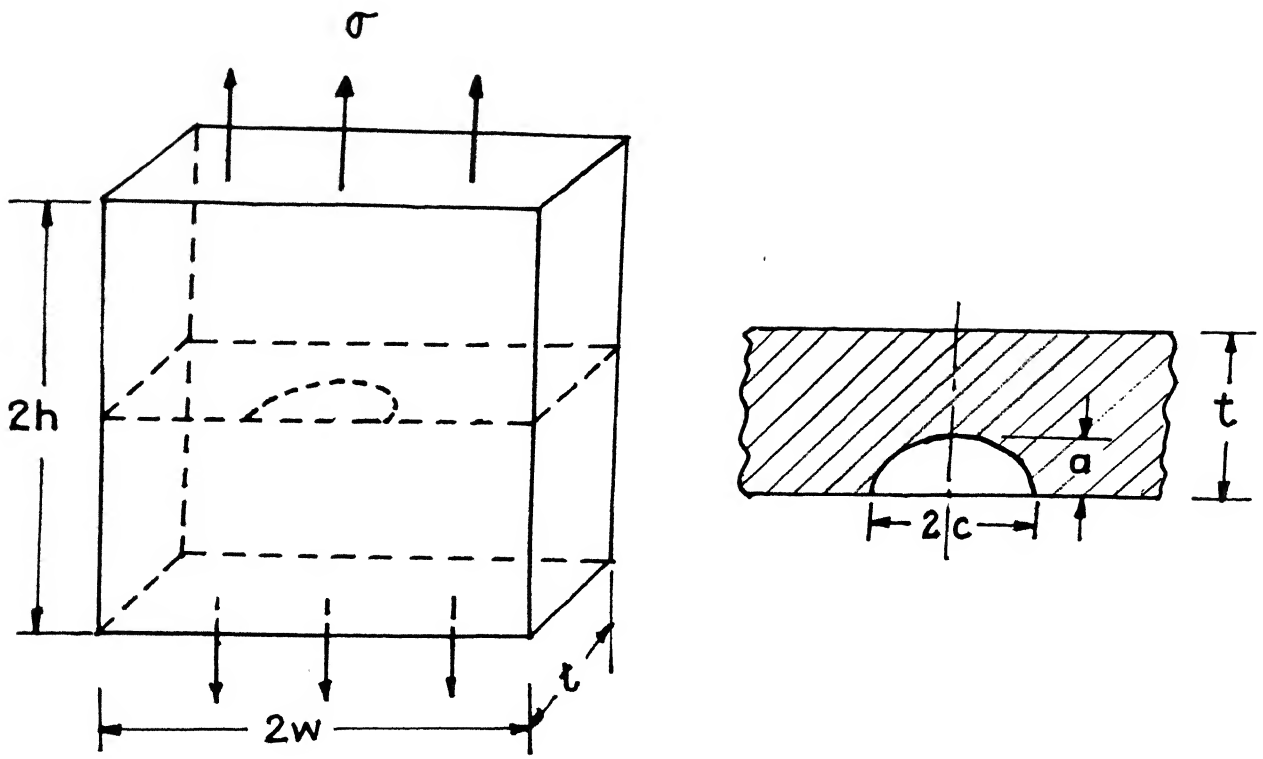

Fig. 4.3d Configuration for Case 4 (not to scale)

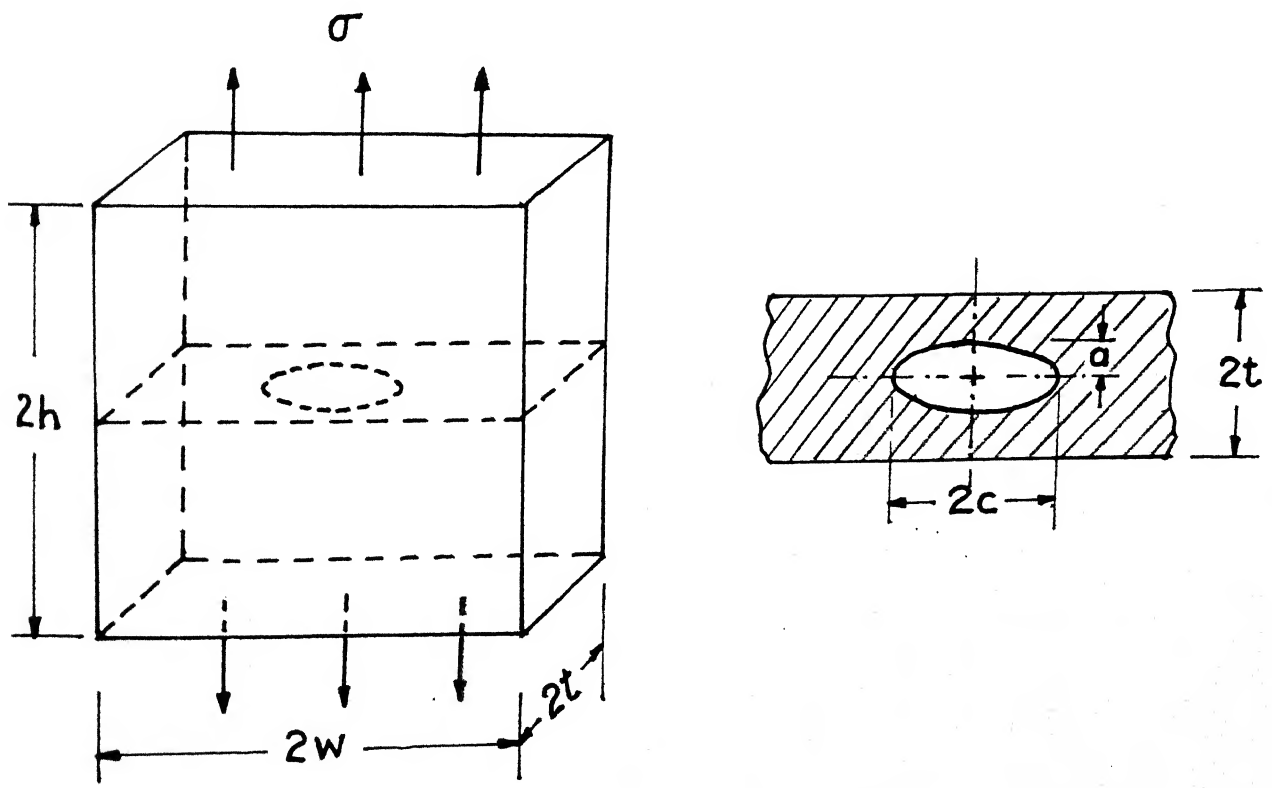

Fig. 4.3e Configuration for Case 5 (not to scale)

CASE 5

An initial elliptical discontinuity is assumed to be embedded inside the plate considered as a three dimensional body (Fig.4.3e). The value for the correction factor, F, is found from empirical relations given in [35]. Two cases, based on the a/b ratio are considered.

1) Elliptical embedded crack with a/b ratio 1.0

The values for a and b are taken as 1.0 mm each. The maximum value of the correction factor is estimated as 0.638. The life estimates are

Initiation life estimate = 2.0×10^{13} cycles

Propagation life estimate = 5.9×10^{5} cycles

Total life estimate = 2.03×10^{13} cycles

2) Semi-circular embedded crack with a/b ratio 2.0

The values of a and b are taken to be 1.0 mm and 0.5 mm respectively. The correction factor, F, is found to be 0.58. The life estimates are

Initiation life estimate = 0.76×10^{13} cycles

Propagation life estimate = 0.78×10^{5} cycles

Total life estimate = 0.76×10^{13} cycles

As in Cases 1 and 2, a comparison between Case 4 and Case 5 reveals that the order of the life estimates is the same irrespective of the location of the flaw.

4.6 EFFECT OF VARIATION OF INITIAL FLAW SIZE ON LIFE ESTIMATES

As seen in the earlier section that for a given loading condition, it is the flaw size that plays a crucial role in estimating the total life. A level of uncertainty can always be expected with any flaw detection technique while taking a value as initial flaw size for a new undamaged blade. With this in view the effect of initial flaw size has been studied.

Case 3 in the previous section is adopted for illustration. The width of the plate is 3.8 cm and its thickness 1.0 cm. The mean and alternating stresses taken for this illustrative case are 99.6 MPa and 560.0 MPa respectively. The values for life estimates with crack sizes varying from 0.25 mm to 1.5 mm are tabulated in Table 4.2 .

It is seen that the initiation life increases with increasing flaw size. This is due to the fact that with an increase in flaw radius there is a lowering of the stress concentration factor. Once initiated, a larger flaw can be seen to propagate more rapidly to failure.

4.7 COMPARISON OF LIFE ESTIMATES BY THE PRESENT METHOD AND THE S-N APPROACH

A comparison is made between the present method and the S-N approach (using the Bagci's failure surface) as used by Rao and Vyas [1].

4.7.1 BAGCI'S FATIGUE FAILURE SURFACE LINE

Bagci's fatigue surface line is of the fourth order and is given

TABLE 4.2

VARIATION OF INITIAL CRACK SIZE ON LIFE ESTIMATES

INITIAL CRACK SIZE (mm)	K_t	N_i (cycles)	N_p (cycles)	N_t (cycles)
0.25	3.00	356	174	530
0.50	2.95	378	134	512
0.75	2.93	388	113	501
1.00	2.90	402	98	500
1.25	2.85	429	88	517
1.50	2.81	452	79	531

by

$$\sigma_{af} = \sigma_e \left(1 - \left[\frac{\sigma_{mf}}{S_y} \right]^4 \right) \qquad (4.24)$$

The S-N plane reads

$\log S_e' = - A \log N + B$ for $10^3 < N < 10^6$

$S_e' = S_e = k S_u$ for $N > 10^6$

with

$$A = \frac{1}{3} \log \left(0.9 \frac{S_u}{S_e} \right)$$

$$B = \log \left(R_f \frac{(0.9 S_u)^2}{S_e} \right)$$

$k = 0.5$ for a standard rotating beam fatigue specimen made of steel.

R_f, the endurance limit modifying factor, is given by

$R_f = K_a K_b K_c K_d K_e K_f$

where

K_a : surface factor

K_b : size factor

K_c : reliability factor

K_d : temperature factor

K_e : stress concentration factor

K_f : miscellaneous effects factor

4.7.2 RESULT

The blade material properties listed in Table 4.1 are used for comparison. It is assumed that a notch of radius 1.0 mm exists in the blade and the configuration corresponds to Fig.4.3c. The theoretical stress concentration factor for this geometry is found to be 2.79 (from Peterson's curves). The alternating stress and the

mean stress values used for the comparison are 85 MPa and 16 MPa respectively.

The value of R_f computed is 0.113, based on suitable values of the modifying factors. The life estimate using the Bagci's fatigue surface line is found to be 0.96×10^5 cycles.

By the strain-life - fracture mechanics combination approach the life estimate obtained is

Initiation life estimate = 5.6×10^{10} cycles

Propagation life estimate = 6632.8 cycles

Total life estimate = 5.6×10^{10} cycles

It can be seen that the S-N approach gives a life lower than that obtained from the present combination approach, since it does not specifically account for the development of the plastic zone and directly assumes an initiated crack which propagates to failure.

4.8 CLOSURE

In this chapter, a combination approach to fatigue life estimation, based on the concepts of strain life and fracture mechanics, is outlined and its use illustrated for the estimation of fatigue life of turbine blades subject to alternating stresses due to nozzle excitation.

CHAPTER 5

C O N C L U S I O N S

In this study the dynamic stress analysis of a typical tapered, twisted, asymmetrical aerofoil cross-section blade mounted on a disc rotating at a constant angular velocity has been undertaken. Stress analysis has been carried out for a blade with nonlinear damping properties. Damping has been defined as a function of mode of vibration, rotor speed and amplitude of vibration, and, a numerical procedure developed for incorporation of such damping in analysis has been presented. Results, obtained for illustrative cases, are presented as functions of rotor speed, excitation harmonics and blade length.

A life prediction algorithm, duly incorporating crack initiation and crack propagation phenomenon, has been developed as an improvement on existing conventional stress based approaches. The algorithm developed is based on the Combination Approach, whereby crack initiation life is appropriately estimated using Strain-Life Methodology while crack propagation life is estimated employing Fracture Mechanics Concepts.

The stress analysis code along with the life estimation algorithm forms the overall package. However, a comprehensive package would require as input the complete stress loading biography of the

blade. Blade histories would involve constant speed service operations along with variable speed operations as during the process of start-up and shut-down of the turbomachine. This study has restricted itself to constant speed rotor operations. Stress Estimation under nonlinear damping during variable speed operations like start-up/shut-down can be taken up as the next stage of analysis. Provision also needs to be made for incorporation of thermal stresses incurred by the blading during operation of the turbomachine.

Life Prediction models are generally constrained in absence of experimental validation. Such validation is considered to be prohibitively expensive. However, there has been a strongly felt need to correlate already occurred blade failures to their loading histories. Collection of such real life blade data from user industries is essential to check upon the efficiency of a proposed failure prediction model.

REFERENCES

[1] Rao, J.S., and Vyas, N.S., " On Life Estimation of Turbine Blading ", Proc. Rotor Dynamics Tech. Comm., Seventh IFToMM World Congress, Sevilla, Spain, 1986.

[2] Rao, J.S., " Turbomachine Blade Vibration ", Shock Vib. Dig., 15(5), p. 3, 1983.

[3] Carnegie, W., Sterling, C. and Fleming, J., " Vibration Characteristics of Turbine Blading under Rotation - Results of an Initial Investigation and Details of a High Speed Test Installation ", paper no. 32, Appld. Mechs. Convention, Cambridge, England, 1966.

[4] Carnegie, W., Dawson, B., and Thomas, J., " Vibration Characteristics of Cantilever Blading ", Proc. I. Mech. E., Vol.180, p. 71, 1966.

[5] Sisto, F. and Chang, A.T., " A Finite Element for Vibration Analysis of Twisted Blades based on Beam Theory ", AIAA Jnl., 422 (11), p. 1646, 1984.

[6] Rawtani, S. and Dokainish, M.A., " Vibration Analysis of Pre-twisted Cantilever Plates ", Trans. CASI, Vol. 2, p. 95, 1969.

[7] Bossack, M.A.J. and Zienkiewicz, O.Z.," Free Vibration of Initially Stressed Solids with particular reference to Centrifugal Force Effects in Rotating Machinery ", Jnl. Strain Analysis, Vol. 8, p.265, 1973.

[8] Leissa, A.W., Macbain, J.C. and Kielb, R.E., " Vibrations of Twisted Cantilever Plates - Summary of Previous and Current Studies ", Jnl. Sound and Vib., 96(2), p. 159, 1984.

[9] Lazan, B.T., **Damping of Materials and Members in Structural Mechanics**, Pergamon Press, NY, 1968.

[10] Hammons, T.J., " Electrical Damping and its effect on Accumulative Fatigue Life Expenditure of Turbine Generator Shafts following Worst Case Supply System Disturbances ", Univ. of Glasgow, U.K., IEEE, 1982.

[11] Rieger, N.F. and Beck, C.M., " Damping Tests on Steam Turbine Blades ", EPRI Project RP-1185-1, Palo Alto, CA, 1980.

[12] Rao, J.S., Gupta, K., Vyas, N.S., " Blade Damping Measurement in A Spin Rig with Nozzle Passing Excitation Simulated by Electromagnets", Proc. Shock Vib. Bull., US Naval Res. Labs.

Proc. 56 , Pt 2, p. 109, 1986.

[13] Rao, J.S., and Vyas, N.S., " Resonant Stress Determination of a Turbine Blade with Modal Damping as a function of Roror Speed and Vibrational Amplitude ", ASME , 89-GT-27.

[14] Rieger, N.F., and Nowak, W.J., " Analysis of Fatigue Stresses in Steam Turbine Blade Groups ", Paper presented at EPRI Seminar Workshop on Stean Turbine Availability, Palo Alto, CA, 1977.

[15] Hoyniak, D. and Fleeter, S., " Prediction of Aerodynamically Induced Vibration in Turbomachinery ", ASME Annual Winter Meeting, p.1, 1981.

[16] Rieger, N.F., " Blade Fatigue ", Proc. Tech. Comm. Rotor Dynamics, Sixth IFToMM Congress, New Delhi, 1983.

[17] Rieger, N.F., " Some Service Problems of Turbine Blades : Factors Affecting Diagnosis and Correction ", Paper presented at EPRI Conf. on NDE of Steam Turbines and Electrical Generator Components, Washington, D.C., 1980.

[18] Rieger , N.F., and Nowak, W.J., " Calculation of Three Dimensional Disk Steeple Stresses ", Consultants' Report to EPRI Nuclear Systems Division, Palo Alto, CA, 1978.

[19] Vyas, N.S., " Vibratory Stress Analysis and Fatigue Life Estimation of Turbine Blade ", Ph.D. Thesis, I.I.T., New Delhi, India, 1986.

[20] Dym, C.L., and Shames, I.H., **Solid Mechanics : A Variational Approach**, McGraw Hill Publication, 1973.

[21] Roark, R.J. and Young, W.C., **Formulas for Stress and Strain**, 5th ed., McGraw Hill IBC, 1976.

[22] Dewey, R.P. and Rieger, N.F., " Survey of Steam Turbine Blade Failures ", Proc. EPRI Workshop on Steam Turbine Availability, Boston, MA, 1982.

[23] Dowling, N.E., " Fatigue at Notches and the Local strain and Fracture Mechanics approaches ", *Fracture Mechanics*, ASTM STP 677, ed. C.W.Smith, p. 247-273, 1979.

[24] Socie, D.F., Dowling, N.E. and Kurath, P., " Fatigue Life Estimation of Notched Members ", *Fracture Mechanics*, 15th Symp., ed. R.J.Sanford, ASTM STP833, p. 284-299, 1984.

[25] Nueber, H., " Theory of Stress Concentration for Shear-Strained Prismatical Bodies with Arbitrary Nonlinear Stress-Strain Laws", J. Appl. Mech., Trans. ASME, Vol. E28, p. 544, 1964.

[26] Massing, G., Proc. 2nd Int. Cong. Appl. Mech., Zurich, 1926.

[27] Morrow, J., **Fatigue Design Handbook**, Advances in Engg., Vol. 4, SAE, Warrendale, Pa., Sec 3.2, p. 21-29, 1968.

[28] Paris, P.C., and Erdogan, F., " A Critical Analysis of Crack Propagation Laws ", Trans. ASME, J. Basic Engg., Vol. D85, p. 528-534, 1963.

[29] Bannantine, J.A., Comer, J.J. and Handrock J.L., **Fundamentals of Metal Fatigue Analysis**, Prentice Hall, Englewood Cliffs, N.J., 1990.

[30] Peterson, R.E., **Stress Concentration Factors**, John Wiley and Sons, New York, 1974.

[31] Basquin, O.H., " The Exponential Law of Endurance Tests ", ASTM Proc., Vol. 10, p. 625-630, 1910.

[32] Coffin, L.F., Jr., " A Study of the Effects of Cyclic Thermal Stresses on a ductile Metal ", Trans. ASME, Vol.76, p.931-950, 1954.

[33] Manson, S.S., " Behaviour of Materials under Conditions of Thermal Stress ", Heat Transfer Symp., Univ. of Michigan, Engg. Res. Inst., p. 9-75, 1953.

[34] Osgood, C.C., **Fatigue Design**, 2nd ed., Pergamon Press, Oxford, 1982.

[35] Murakami, Y., (ed.- in - chief), **Stress Intensity Factors Handbook**, Vol. 1 and 2, Pergamon Press, 1987.

[36] Rao, J.S., **Turbomachine Blade Vibration**, Wiley Eastern Limited, 1991.